Dead-Reckoning Animal Movements in R – A Reappraisal Using Gundog.Tracks

Richard Michael Gunner (792021@swansea.ac.uk)
Swansea University https://orcid.org/0000-0002-2054-9944

Mark D Holton
Swansea University Department of Biosciences

Mike D Scantlebury
Queen's University Belfast School of Biological Sciences

Louis van Schalkwyk
South Africa Department of Rural Development and Land Reform. State Veterinarian

Holly M English
University College Dublin School of Biology and Environmental Science

Hannah J Williams
Max Planck Institute of Animal Behavior: Max-Planck-Institut fur Verhaltensbiologie

Phil Hopkins
Swansea University Department of Biosciences

Flavio Quintana
Instituto de Biologia de Organismos Marinos (IBIOMAR), CONICET

Agustina Gómez-Laich
Institute of Ecology, Genetics and Evolution. Buenos Aires (IEGEBA) CONICET-UBA

Luca Börger
Swansea University Department of Biosciences

James Redcliffe
Swansea University Department of Biosciences

Ken Yoda
Nagoya University Graduate School of Medicine Faculty of Medicine: Nagoya Daigaku Daigakuin Igakukei Kenkyuka Igakubu

Takashi Yamamoto
Organization for the Strategic Coordination of Research and Intellectual Properties, Meiji University

Sam Ferreira
SANParks: South African National Parks. Scientific Services

Danny Govender
SANParks: South African National Parks

Pauli Viljoen
SANParks: South African National Parks. Scientific Services

Angela Bruns
SANParks: South African National Parks. Veterinary Wildlife Services
Stephen H Bell
Queen's University Belfast School of Biological Sciences
Nikki Marks
Queen's University Belfast School of Biological Sciences
Nigel C Bennet
University of Pretoria Department of Zoology and Entomology
Mariano H Tonini
Instituto Andino Patagonico de Tecnologias Biologicas y Geoambientales. IPATEC-UNICO-CONICET
Carlos M Duarte
CBRC: King Abdullah University of Science and Technology Computational Bioscience Research Center
Martin C van Rooyen
University of Pretoria Department of Zoology and Entomology
Mads F Bertelsen
Center for Zoo and Wild Animal Health, Copenhagen Zoo
Craig J Tambling
University of Fort Hare Department of Zoology and Entomology
Rory P Wilson
Swansea University Department of Biosciences

Research

Keywords: Animal behaviour, Animal movement, Global Positioning System, R (programming language), Track integration, Tri-axial accelerometers, Tri-axial magnetometers

Posted Date: March 19th, 2021

DOI: https://doi.org/10.21203/rs.3.rs-311276/v1

Version of Record: A version of this preprint was published at Animal Biotelemetry on July 1st, 2021. See the published version at https://doi.org/10.1186/s40317-021-00245-z.

Dead-reckoning animal movements in R – A reappraisal using *Gundog.Tracks*

Running title: Animal dead-reckoning in R

Richard M. Gunner[1*], Mark D. Holton[1], Mike. D Scantlebury[2], O. Louis van Schalkwyk[3,4,5], Holly M. English[6], Hannah J. Williams[5], Phil Hopkins[1], Flavio Quintana[7], Agustina Gómez-Laich[8], Luca Börger[1,9], James Redcliffe[1], Ken Yoda[10], Takashi Yamamoto[11], Sam Ferreira[12], Danny Govender[12], Pauli Viljoen[12], Angela Bruns[13], Stephen H. Bell[2], Nikki J. Marks[2], Nigel C. Bennett[14], Mariano H. Tonini[15], Carlos M. Duarte[16], Martin V. Rooyen[14], Mads F. Bertelsen[17], Craig J. Tambling[18], Rory P. Wilson[1]

[1]Swansea Lab for Animal Movement, Biosciences, College of Science, Swansea University, Singleton Park, Swansea, Wales SA2 8PP, United Kingdom
[2]School of Biological Sciences, Queen's University Belfast, Belfast, 19 Chlorine Gardens, Belfast BT9 5DL, Northern Ireland, United Kingdom
[3]Department of Agriculture, Land Reform and Rural Development, Government of South Africa, Pretoria, 001, South Africa
[4]Department of Migration, Max Planck Institute of Animal Behavior, 78315 Radolfzell, Germany
[5]Department of Veterinary Tropical Diseases, Faculty of Veterinary Science, University of Pretoria, Onderstepoort, 0110, South Africa
[6]School of Biology and Environmental Science, University College Dublin, Belfield, Dublin, Ireland
[7]Instituto de Biología de Organismos Marinos (IBIOMAR), CONICET. Boulevard Brown 2915, U9120ACD, Puerto Madryn, Chubut, Argentina
[8]Departamento de Ecología, Genética y Evolución & Instituto de Ecología, Genética y Evolución de Buenos Aires (IEGEBA), CONICET, Pabellón II Ciudad Universitaria, C1428EGA, Buenos Aires, Argentina
[9]Centre for Biomathematics, College of Science, Swansea University, Swansea SA2 8PP, UK
[10]Graduate School of Environmental Studies, Nagoya University, Furo-cho, Chikusa-ku, Nagoya, Japan
[11]Organization for the Strategic Coordination of Research and Intellectual Properties, Meiji University, Nakano, Tokyo, Japan
[12]Savanna and Grassland Research Unit, South African National Parks, Scientific Services Skukuza, Kruger National Park, Skukuza, 1350, South Africa
[13]Veterinary Wildlife Services, South African National Parks, 97 Memorial Road, Old Testing Grounds, 8301, Kimberley, South Africa
[14]Mammal Research Institute. Department of Zoology and Entomology, University of Pretoria, Pretoria, 002. South Africa
[15]Instituto Andino Patagónico de Tecnologías Biológicas y Geoambientales, Grupo GEA, IPATEC-UNCO-CONICET, San Carlos de Bariloche, Río Negro, Argentina
[16]Red Sea Research Centre, King Abdullah University of Science and Technology, Thuwal 23955, Saudi Arabia
[17]Center for Zoo and Wild Animal Health, Copenhagen Zoo, Roskildevej 38, DK-2000, Frederiksberg, Denmark
[18]Department of Zoology and Entomology. University of Fort Hare Alice Campus, Ring Road, Alice, 5700, South Africa

*** Correspondence:**
Richard M. Gunner
richard.m.g@hotmail.com

Keywords: Animal behaviour, Animal movement, Global Positioning System, R (programming language), Track integration, Tri-axial accelerometers, Tri-axial magnetometers

Abstract

Background

Fine-scale data on animal position are increasingly enabling us to understand the details of animal movement ecology and dead-reckoning, a technique integrating motion sensor-derived information on heading and speed, can be used to reconstruct fine-scale movement paths at sub-second resolution, irrespective of the environment. On its own however, the dead-reckoning process is prone to cumulative errors, so that position estimates quickly become uncoupled from true location. Periodic ground-truthing with aligned location data (e.g., from global positioning technology) can correct for this drift between Verified Positions (VPs). Yet relatively few bio-logging studies have adopted this approach due to an apparent inaccessibility of the complex analytical processes involved. We present step-by-step instructions for implementing Verified Position Correction (VPC) dead-reckoning in R using the tilt-compensated compass method, accompanied by the mathematical protocols underlying the code and improvements and extensions of this technique to reduce the trade-off between VPC rate and dead-reckoning accuracy. These protocols are all built into a user-friendly, fully-annotated VPC dead-reckoning R function; *Gundog.Tracks*, with multi-functionality to reconstruct animal movement paths across terrestrial, aquatic, and aerial systems, provided within the supplementary information as well as online (GitHub).

Results

The *Gundog.Tracks* function is demonstrated on three contrasting model species (the African lion *Panthera leo*, the Magellanic penguin *Spheniscus magellanicus*, and the Imperial cormorant *Leucocarbo atriceps*) moving on land, in water and in air, respectively. We show the effect of uncorrected errors in speed estimations, heading inaccuracies and infrequent VPC rate and demonstrate how these issues can be addressed.

Conclusions

The function provided will allow anyone familiar with R to dead-reckon animal tracks readily and accurately, as the key complex issues are dealt with by *Gundog.Tracks*. This will help the community to consider and implement a valuable, but often overlooked method of reconstructing high-resolution animal movement paths across diverse species and systems without requiring a bespoke application.

1. Background

Reconstructing animal movement paths is an important tool in ecology, providing insights into animal space use, behaviour and habitat selection. However, accurate estimation of paths at fine temporal scales has proved a persistent challenge [1, 2]. Dead-reckoning is a method used to reconstruct animal movement paths, based on sequentially integrating the vector of travel from a predetermined position using estimates of heading (also termed 'bearing' or 'yaw') and velocity (and displacement about the vertical axis for 3-D movements), over an elapsed time interval [3-6]. In its most advanced form, it can provide positional data with sub-second resolution, irrespective of the environment [e.g., 7, 8, 9] and it therefore has huge potential for providing data that can elucidate many fundamental behavioural and ecological issues related to space-use.

The concept of dead-reckoning (also termed 'track integration') originated to aid nautical navigation [3, 10], though its utility to reconstruct uninterrupted fine-scale (in time and space) animal movement paths by integrating different sensors in animal-attached tags was suggested over three decades ago [11, 12]. Today, this typically involves the simultaneous deployment of tri-axial accelerometers and magnetometers [e.g., 6, 7, 13, 14-17], utilising the tilt-compensated compass method [cf. 18, 19-21].

The utility of dead-reckoning depends on the accuracy of speed and heading estimates (see Table. 1) and, due to the nature of vector integration, dead-reckoned tracks accumulate errors (commonly termed 'drift') over time [12, 22, 23]. As a result, periodic ground-truthing by a secondary source is important for maintaining the accuracy of animal paths with all its underlying scales and tortuosity of movement [6, 7, 24]. For this reason, dead-reckoning data is normally enhanced by combining it with other methods for providing verified positions

(VPs). These are primarily; direct observation [e.g., 25], light intensity-based geolocation [e.g., 26], VHF- [e.g., 27], acoustic- [e.g., 28] and GPS telemetry [e.g., 23]. Other, less utilised, systems that may also have merit at sites frequented by the tagged animals, include radio frequency identification (RFID) stations [cf. 29], camera traps [cf. 30] and video footage, such as closed-circuit television (CCTV) surveillance [e.g., 31]. Although all these systems are subject to a number of issues that can make their positional fixes temporally widely spaced [e.g., 1, 32, 33], inaccurate [e.g., 34, 35, 36] or impossible [e.g., 37, 38, 39], they can be critical in providing ground-truthed positions, even infrequently, with which to reset accumulated drift [6, 23].

Of the above VP options, GPS-corrected dead-reckoning is the most widely used and there is a marked bias towards marine studies [e.g., 7-9, 12-14, 16, 24, 40, 41-53]. This is likely because speed can be more easily measured or approximated in water, with previous studies obtaining estimates *via* acoustic flow noise [e.g., 54], passive sonar [e.g., 55], pitch and change in depth [e.g., 8] and speed sensors [cf. 13, 56, 57]. The efficacy of such techniques diminishes within the aerial environment, principally, due to the marked difference between water and air density [cf. 58] and the current strength and volatility of wind [cf. 59, 60]. Indeed, this may explain why, in part, (to our knowledge) only one study to date has dead-reckoned a volant species [61]. More recently, dynamic body acceleration (DBA, see Wilson et al. [62], for recent review) has been validated as a proxy of speed for terrestrial animals [63, 64] although there are still very few studies that use the dead-reckoning method in terrestrial animals [e.g., 6, 7, 23, 31, 65, 66].

Table 1. Possible system errors that can affect the utility of animal dead-reckoning within the 'tilt-compensated compass' framework. 'SI' refers to Supplementary information.

System error	Reasons for error	Underlying causes	References	Possible mitigation measures
Derived Heading	Erroneous static acceleration (postural) estimates	During bouts of high centripetal (turning) acceleration	[67] [68] [69] [60] [70]	Gyro-integrated data [cf. 71, 72]
	Using Euler angles (angle of rotation about each axis of a given coordinate system)	The orientation of the device with respect to the earth's frame of reference (cf. SI_2) can only be defined reasonably at angles less than perpendicular or less than a 180° inversion (dependent on pitch & roll equations used - cf. Section 3) from their longitudinal and lateral axes of 'normal' posture (otherwise, unstable measures arise from the Gimbal lock singularity complex [cf. 73], whilst x, y and z values can become inversed and/or represent different 'surge', 'sway' and 'heave' planes)	[74] [75] [76] [18] [77]	Quaternion-estimated heading [cf. 78, 79, 80]
	Tag placement/ dislodgment	In line with the above - range for accurate angular (pitch & roll) measures are restricted in one or more dimensions Heading will be biased according to the degree of displacement about the z-axis	[16] [81]	Ensure tag orientation is noted during deployment and retrieval operations (and subsequently used in corrections)
	Variations in the strength and declination of magnetic fields	Animals that undertake long journeys (regionally/globally) Environmental and man-made magnetic noise (iron distortions)	[82]	Ensure at least one magnetic calibration procedure is carried out (see SI_3 for details) and apply magnetic declination offset to heading values where required
Derived Speed	Deviations of the DBA~speed relationship	Load bearing Moving over a deformable substrate / changeable incline Changing gait Moving within fluid media	[83] [84] [85] [63] [64] [86] [9]	Iteratively modulate the gradient and/or intercept within the DBA~speed linear regression according to environmental circumstance and mode of movement [cf. 63]. By-pass DBA (e.g., use speed/acoustic sensors, step/tail-/wing beat frequency, vertical speed etc. [e.g., 44])
Both	External forces (e.g., current vectors in air- and water flow)	Decreases the signal-to-noise ratio of motion sensor data. Affects the relationship between an animal's (longitudinal axis) direction of travel from their true vector of travel Some animals do not always move in the same direction as their anterior-posterior axis	[12] [43] [87] [8]	Smooth postural (and pre-derivative data) / DBA estimates [cf. 62] Incorporate current flow vectors within the dead-reckoning procedure

We suggest that a primary reason that Verified Position Correction (VPC) dead-reckoning has been little used relates to the apparent difficulty and poor accessibility of the analytical processes involved. With this in mind, the primary aim of this paper is to provide potential users with a clear, concise roadmap for implementing dead-reckoning protocols. Specifically, we revisit the dead-reckoning methodology, from calibrating magnetometry data and deriving heading (tilt-compensated compass method), to VPC dead-reckoning within both terrestrial and fluid media. We provide simplistic conceptual explanations and mathematical protocols and describe the pitfalls within the procedure that can increase error. We also translate the relevant equations into complementary R code [cf. 88, available at 89] throughout the text, with fully annotated scripts deposited in the supplementary information (SI) and GitHub [available at 90].

In addition to the above, we outline recent advances to the VPC dead-reckoning technique. For use in terrestrial environments, this includes implementing step counts as a distance measure, by-passing dynamic body acceleration (DBA) as a proxy of speed, and assessing the value of 'reverse dead-reckoning' (useful when VPs are concentrated to the latter end of an animal's trajectory). For marine and aerial environments, we demonstrate the value of integrating tidal-/air current data with dead-reckoned vectors (hereafter termed 'current integration') to reduce errors attributed to drift [cf. 43, 87]. Across all three media of travel (land, water and air), we show the value of incorporating different speed coefficients according to behaviour types. In addition, we provide examples of the various methods by which VP data can be under-sampled (relevant for high-res GPS datasets) prior to correcting dead-reckoned tracks and discuss the scales at which users should consider VP correction (which depend on the details of species-specific movement and length of data acquisition). We specifically demonstrate the above using our R-functions (*Gundog.Tracks* being the

primary function for dead-reckoning), providing examples of its utility across various scenarios. Lastly, we highlight the relevance of heading and distance correction factors (derived from the VPC procedure), which can also be used to interrogate the animal-environment interaction and biases stemming from animal tag performance.

To illustrate our approach, we use three model species (the African lion *Panthera leo*, the Magellanic penguin *Spheniscus magellanicus* and the Imperial cormorant *Leucocarbo atriceps*) that cover almost two orders of size magnitude in body mass and that operate in markedly different environments and at different scales of movement. To make this review more broadly applicable to researchers of varying dead-reckoning and R knowledge, we have departed from a traditional article format and instead, split this body of work into two distinct sections: Firstly, we provide an overview of the critical *Gundog.Tracks* function and provide a brief review of the conceptual workflow (Section 2). With respect to this, we discuss the relevant strengths and limitations of the current dead-reckoning framework and the key considerations involved. Secondly, we detail each 'potential' stage of the VPC dead-reckoning procedure with exemplar mathematical equations and R syntax (Section 3).

2. Implementation of *Gundog.Tracks*

2.1 User functionality

Gundog.Tracks is an all-encompassing dead-reckoning function that can be used to dead-reckon animal paths travelling terrestrially or through fluid media. User-defined inputs can specify a combination of procedures (elaborated below), including: (i) Reverse dead-reckoning, (ii) Integrating travel and current vectors and, if supplied, the method and degree of VP under-sampling prior to correction (cf. Table 2). The user can opt to derive speed using the DBA approach, with multi-functionality to modulate (iii) DBA~speed relationships. Conversely, in cases where DBA is a weak proxy of speed, the user can supply (iv) Pre-determined speed data. The function's method of (v) VPC, automatically handles *NaN* and Infinite (*Inf*) values which can arise during the derivation of the distance correction factors (detailed within Section 3). Table 2 details all the function's input requirements/options.

<u>Reverse dead-reckoning</u>

Dead-reckoning backwards is useful when the start position is unknown, but the finishing coordinates are known. For example, central-place foraging, diving animals returning to land from the sea may not acquire a satellite fix for an appreciable period of time following submersion in water which can make determining the start position difficult. So, when VPs are skewed to the latter part of the track, it may be beneficial to start the iterative dead-reckon process from that end. This involves reversing the order of data to be dead-reckoned and changing heading values by 180 degrees prior to dead-reckoning.

Integrating current vectors

Wind or ocean currents can change the relationship between an animal's (longitudinal axis) bearing and speed of travel from their true vector of travel [43, 87]. This drift can be incorporated within movement paths by advancing each iterated dead-reckoned vector according to the direction and speed of the current at that point in space and time (cf. Fig. 1).

DBA~speed derivation

Given the approximate linear relationship between DBA *[sensu 62]* and terrestrial animal speed, DBA estimates can be multiplied by a gradient, *m* and summed with an intercept, *c* to derive speed [7, 23], which are typically substituted with results from DBA~speed linear regression estimates [23, 64, 91, 92]. The *m* coefficient should be selected such that (uncorrected) dead-reckoned tracks accord with the apparent straight-line distance between VPs. Importantly, the DBA~speed relationship may be a function of terrain-type (e.g., sand *vs* concrete), animal state (e.g., weight variation) and mode of movement (e.g., running *vs* climbing) [cf. 63]. For instance, a condor gliding within a thermal would have high speeds, despite having negligible DBA, while an Ibex traversing across different substrate types and gradients would impart varying magnitudes of acceleration that may scale non-linearly with a change in stride gait. It may be of value, therefore, to iteratively change the supplied *m* (and possibly *c*) values between VPs according to behaviour and environment. The user may also opt to supply a 'marked events' (*ME*) vector (a marked event refers to a number of sequential (in time) data points within a dataset coded for with integer values) to ensure dead-reckoned tracks are not advanced with non-translational behaviours. Within *Gundog.Tracks*, *ME* values of one or greater reflect progressive movement, and zero values code for stationary

behaviour - e.g., in its simplest form, *ME* could be filled with binary 0's and 1's as governed by a DBA threshold (labelling the *ME* vector 0 in sleep and resting behaviour).

Pre-determining speed

For terrestrial species (specifically bipeds and quadrupeds), the interplay between peak heave acceleration amplitude and periodicity may be a useful indicator for the movement gait adopted [93], which may help decide the coefficient multiplier in the DBA~speed relationship [64]. There may be times, however, when DBA is an unreliable proxy of terrestrial speed [cf. 63]. At this time, given that the stride cycle can be easily detected by cyclic peaks in a given acceleration channel [e.g., 94, 95, 96], peak periodicity (and amplitude) may be used as a proxy of distance moved by providing a distance per step estimate (assuming constant distance travelled between step gaits if only concerning step periodicity- cf. Section 3 and SI_4).

DBA is a weak proxy of speed for many marine animals because associated air volumes change upthrust with depth so that speed may be invariant of the movement kinematics [cf. 97]. DBA is also a weak proxy for flying animals that glide at constant velocity, use thermals or bank [cf. 98]. One of the most common methods for determining animal speed in water is *via* devices that estimate flow or resistance rate [13, 16, 59, 99]. These often have appreciable limitations, with currents, biofouling, blockage and turbulence affecting performance [59], and many of these issues are applicable to volant species, so that bird speed measures are typically restricted to GPS-derived estimates of ground speed [cf. 100]. In the absence of a reliable motion sensor-derived speed proxy, previous reported approximated speed estimates according to movement modes and/or topological whereabouts can be used [cf. 27]. For example, for various diving animals such as penguins, a simple depth threshold may prove

effective to differentiate between various previous reported modal ‘surface-resting‘ and ‘underwater-commuting’ speeds [56, 101-103]. For volant species, whilst wingbeat frequency or amplitude does not scale reliably with air speed [cf. 104], the interplay between both can decipher various flight modes (e.g., ‘cruising speed’ *vs* taking off/landing) [60, 105]. Furthermore, tail beat frequency has been shown to be a good predictor of swimming speed for various fish species [106-108]. For diving animals, a proxy for horizontal speed can be obtained based on animal pitch and rate of change of depth [8, 109]. Specifically, the rate change of depth is divided by the tangent of the body pitch.

In any case, when high resolution VP data is available (e.g., 0.01-10 Hz GPS), for instance, during short-term trial deployments, speed estimates can be compared alongside those derived between VPs and approximated according to behaviour type (elucidated from, for example, accelerometery- [e.g., 110, 111], magnetometry- [e.g., 98, 112]), depth- [e.g., 113] or altitude- [e.g., 60] data, and uncorrected dead-reckoned tracks can be compared alongside VPs to determine where biases may occur visually. Furthermore, the correction factors obtained from the VPC process are viable comparators for detecting consistent under- or over-estimations of speed and/or heading offsets (e.g., due to tag placement). Speed values can then be iteratively adjusted until uncorrected dead-reckoned tracks match their aligned ground-truthed positions. Within *Gundog.Tracks*, the user can modulate *m*, *c* and *ME* values to switch between pre-determined speed ($m = 1$, $c = 0$), DBA derived speed ($m > 0$, $c \geq 0$) and stationary behaviour ($ME = 0$).

VPC procedure

Ground-truthing dead-reckoned tracks typically involves the linear drift correction method [cf. 23, 43], outlined in Constandache et al. [114] & Symington and Trigoni [115]. In essence, a shift vector aligns the starting dead-reckoned path segment with the VP at time point one, after which the difference between the VP and dead-reckoned path segment at time point two is calculated to provide a correction vector that is applied linearly between time point one and time point two. Our method follows the protocols outlined by Walker et al. [6], whereby the underlying correction coefficients (hereafter termed 'factors') for both heading and (radial) distance are calculated - adjusting the length and heading at each dead-reckoned path segment until the end points align to each VP along the path. This process requires the trigonometric 'as the crow flies' Haversine formulae [116-118] which allows one to translate a distance across the curvature of the Earth's surface (detailed within Section 3). The advantage of this method is that, whilst correction factors are constant between VPs, it does not assume that the dead-reckoned path deviates linearly over time from the true path because (radial) distance is multiplied by the distance correction factor. This ensures that parts of track where the animal is determined to be stationary (e.g., $ME = 0$) are left unaltered. It is worth noting that even animals that travel in 3-D can be subject to the 2-D dead-reckoning formulae and Haversine computation of distance correction factors because we typically assume that both dead-reckoned- and VP positions are aligned in vertical space (assuming reliable pressure- [60]/ depth [13] data) and attempt to control for the horizontal component of speed (e.g., Section 3 - $E_{14,16}$) pre-correction. Although not covered here, we acknowledge that various state-space modelling techniques have also been developed to georeference dead-reckoned tracks [e.g., 8, 44].

Table 2. Gundog.Tracks input fields and description of their role. Ref refers to the default value when no input is stated. Red shading represents required user inputs and green and orange shading reflect optional inputs (the latter change when using VPC). Note that if speed estimates (v) are directly inputted into the function then m, c and ME defaults should not be changed. If either one of the VP.lon, VP.lat or method inputs is specified as NULL, then no VPC will occur.

Function input	Description	Ref
TS	Timestamp - POSIXct object. No missing data (NA's) permitted	-
h	Heading (0° to 360°) - No missing data (NA's) permitted	-
v	DBA (*g* or m/s^2) or speed (m/s) - No missing data (NA's) permitted	-
elv	Elevation / depth data (m) - No missing data (NA's) permitted	0
p	Pitch (°) – Only supply if user wants radial distance modulated according to pitch (cf. section 3 - E_{16}). No missing data (NA's) permitted	NULL
cs	Current strength (m/s) - Supplied as a single value or vector/column of changeable values. NA's are replaced with the most recent non-NA prior to it (observations carried forward)	NULL
ch	Current heading (0° to 360°) - Supplied as a single value or vector/column of changeable values. NA's are replaced with the most recent non-NA prior to it (observations carried forward)	NULL
m	Multiplicative coefficient (gradient) - If speed (m/s) supplied for v, then m must be 1. Supplied as a single value or vector/column of changeable values	1
c	Constant (y-intercept) – If speed supplied for v, then c must be 0. Supplied as a single value or vector/column of changeable values	0
ME	Marked Events – 0 denotes periods of stationary behaviour and 1 (or any integer number > 0) denotes periods of traversing movement. ME overrides initial speed input / DBA-derived speed (calculated within the function itself)	1
lo	Starting longitude coordinate to advance dead-reckon track from – Decimal format, e.g., 26.31989	0
la	Starting latitude coordinate to advance dead-reckon track from – Decimal format e.g., -06.11995	0
VP.lon	VP longitude coordinates – Decimal format. Missing relocation data expressed as either NA's or 0's. First (or last if reverse dead-reckoning) element/row allocated as **lo** within the function	NULL
VP.lat	VP latitude coordinates – Decimal format. Missing relocation data expressed as either NA's or 0's. First (or last if reverse dead-reckoning) element/row allocated as **la** within the function	NULL
VP.ME	TRUE = Supplied VPs removed at times when ME = 0 (relevant for high-res VP datasets, when location error is high during rest). Note, this does not remove the element/row allocated as lo/la	FALSE
method	How the function under-samples VPs prior to correction (subsequent to the VP.ME subset, if set to TRUE) – **"divide"** = Fix kept every *x (thresh)* segments of supplied VPs, based on row number. The first and last fixes are always included **"time"** (s) = Fix kept every *x (thresh*) accumulated seconds (or the next available fix after a period of missing locational data *(≥ thresh).* The first and last fixes are always included **"distance"** = Fix kept every *x (thresh)* proportional segments of the total accumulated distance (m) between supplied VPs (using the stepping interval 'dist.step'). The first and last fixes are always included **"all"** = Every supplied VP kept (irrespective of thresh value)	NULL
thresh	Threshold - Degree of VP under-sampling prior to dead-reckon correction. The frequency of under sampling depends on the method selected	1
dist.step	The stepping interval used for calculating distance between VPs, both within the VP summary distance metrics (see Table. 3) and within the 'method = distance' VP under-sampling protocol prior to VPC. For example, dist.step = 5 computes distance between every 5th VP (irrespective of the time difference between them)	1
bound	TRUE = VPC dead-reckoning is bounded by the first and last VP present FALSE = VPC dead-reckoning is unbounded by the last available VP. The last dead-reckoned track segment inherits the previous correction factors	TRUE
Outgoing	TRUE = 'normal' dead-reckoning procedure FALSE = Reverse dead-reckoning. Note **la** and **lo** positions should now be the finishing longitude and latitude coordinates, respectively	TRUE
Plot	FALSE = No summary plots TRUE = R graphics window initialized: VPC = 4 summary plots / no VPC = 1 summary plot (cf. top left) **Top left)** Uncorrected dead-reckoned track (blue) and VP track (red). If currents are supplied, the blue track has currents integrated and an additional green track with no current integration is plotted **Top right)** VPC dead-reckoned track (blue) in relation to VP track (red) **Bottom left)** Net error (m) between VPs and dead-reckoned positions (un-corrected = red and corrected = black). If currents are supplied, then uncorrected with no current integration = green and uncorrected with current integration = red. **Bottom right)** VPC corrected dead-reckoned track	TRUE

2.2 Default inputs for calculations and outputs

Gundog.Tracks default input takes the form:

Gundog.Tracks(TS, h, v, elv = 0, p = NULL, cs = NULL, ch = NULL, m = 1, c = 0, ME = 1, lo = 0, la = 0, VP.lon = NULL, VP.lat = NULL, VP.ME = FALSE, method = NULL, thresh = 1, dist.step = 1, bound = TRUE, Outgoing = TRUE, plot = FALSE)

, with input modulated according to the animal in question and data available (see Fig. 2).

The function outputs a data frame containing various descriptive columns which, depending on the input, includes (but is not limited to);

- The correction factors used
- Heading and radial distance estimates (both pre- and post-current integration and/or VPC)
- Distance moved and speed estimates (both in 2-D and 3-D when elevation/depth data supplied)
- Net error between dead-reckoned positions and VPs (both pre- and post-correction)
- Various VP summaries including notation of when VPs are present and which fixes were used in the correction process.

When specified, 2-D summary plots demonstrating the relationship between dead-reckoned positions and VPs (both pre- and post-current integration and/or VPC) are provided (e.g., Fig. 3). Table 3 details all the function's available outputs (modulated according to input). *Gundog.Tracks* uses the *na.locf()* function from the '*zoo*' package [119] and the *slice()* function from the '*dplyr*' package [120] (both are checked as dependencies and installed when required within this function). Output 2-D distance/speed estimates are calculated with the

Haversine formula. When depth/elevation data is supplied (and changes between sets of coordinates) 3-D distance/speed estimates are calculated with a variant of the Euclidean Formula - converting x, y, z from polar to Cartesian coordinates, and incorporating the Earth's oblate spheroid (cf. World Geodetic System (WGS84)), *via* conversion from Geodetic- to Geocentric-latitude [cf. 121].

*Table 3. Gundog.Tracks data frame output names and their parameters. The shading of Ref refers to when the outputs occur; red shading = always, purple shading = when pitch data is supplied, green shading = when elevation/depth data is supplied, blue = when current data is supplied and orange = when the user opts to undertake VPC. The symbol * demonstrates that the metrics will be derived from VPC tracks when correction is initialised. Note that, subsequent to reverse dead-reckoning, the data frame is reverted (back to original time order), though observations are carried backwards in some instances, indicated by ↑. Due to the nature of reverse dead-reckoning (cf. SI_6), some input fields are shifted forward one row following the initial inversion of data. As such, fields indicated by #, are one row further forward in time (this is important when relating Head.corr.factor and Heading.corr output to the equivalent (uncorrected) Heading output. However, when currents are integrated, the Head.corr.factor and Heading.corr outputs refer to Heading.current.integrated and these are synchronized row-wise. All heading related data are rotated back 180 degrees following reverse dead-reckoning.*

Function output	Description	Ref
Row.number	Row number	
Timestamp	Supplied timestamp - POSIXct object	
DR.seconds	Accumulated time (s) based on the supplied timestamp	
Heading	Supplied heading (0° to 360°)	
Marked.events	Supplied Marked events (or replicated default)	
DBA.or.speed	Supplied DBA (*g* or m/s^2) or speed (m/s)	
Pitch	Supplied pitch (°)	
Radial.distance	The calculated q coefficient (prior to VPC) (cf. Sector 3 - E_{15})	#
Elevation	Supplied elevation / depth (m)	
Elevation.diff	Rate change of supplied elevation/depth (m/s) - (elevation difference / time difference between rows)	
Current.strength	Supplied current strength (m/s)	
Current.heading	Supplied current heading (0° to 360°)	
Heading.current.integrated	Updated heading (0° to 360°) following addition of current vectors (prior to VPC)	#
Radial.distance.current.integrated	Updated q coefficient following addition of current vectors (prior to VPC)	#
DR.longitude	Dead-reckoned longitude coordinates – Decimal format (prior to VPC)	
DR.latitude	Dead-reckoned latitude coordinates – Decimal format (prior to VPC)	
DR.longitude.corr	Corrected dead-reckoned longitude coordinates – Decimal format (post VPC)	
DR.latitude.corr	Corrected dead-reckoned latitude coordinates – Decimal format (post VPC)	
Dist.corr.factor	Distance correction factor (observations carried forward)	↑ #
Head.corr.factor	Heading correction factor (0° to 360°) (observations carried forward)	↑ #
Heading.corr	Corrected heading (0° to 360°) (post VPC)	#
Radial.distance.corr	Corrected q coefficient (post VPC)	#

Distance.error.before.correction	Distance (m) between uncorrected dead-reckoned positions and VPs (observations carried forward), subsequent to sub-sampling according to ME, if VP.ME = TRUE	↑
Distance.error.after.correction	Distance (m) between corrected dead-reckoned positions and VPs (observations carried forward), subsequent to sub-sampling according to ME, if VP.ME = TRUE	↑
DR.distance.2D	Two-dimensional distance moved (m) between dead-reckoned fixes	*
DR.distance.3D	Three-dimensional distance moved (m) between dead-reckoned fixes	*
DR.cumulative.distance.2D	Accumulated two-dimensional distance moved (m) between dead-reckoned fixes	*
DR.cumulative.distance.3D	Accumulated three-dimensional distance moved (m) between dead-reckoned fixes	*
DR.distance.from.start.2D	Two-dimensional (straight-line) distance moved (m) from starting position	*
DR.distance.from.start.3D	Three-dimensional (straight-line) distance moved (m) from the starting position	*
DR.speed.2D	Horizontal speed (m/s) (DR.distance.2D / time difference between rows)	*
DR.speed.3D	Total speed (m/s) (DR.distance.3D / time difference between rows)	*
VP.seconds	Accumulated time (s) between supplied VPs (observations carried forward)	
VP.longitude	Supplied VP longitude values (observations carried forward), sub-sampled according to ME, if VP.ME = TRUE	↑
VP.latitude	Supplied VP latitude values (observations carried forward), sub-sampled according to ME, if VP.ME = TRUE	↑
VP.fix.present	Denotes when a fix was present (1) or absent (0), subsequent to sub-sampling according to ME, if VP.ME = TRUE	
VP.used.to.correct	Denotes which VPs were used to correct (1) and which VPs were ignored (0)	
Number.of.VPCs	Increments by 1 each time a VP was used to correct (observations carried forward)	↑
VP.thresh	Replicates the thresh value set (or default) or warns the user that additional VP under-sampling was required if 'Inf' values produced	
VP.distance.2D	Two-dimensional distance moved (m) between VPs,), subsequent to sub-sampling according to ME, if VP.ME = TRUE and using the stepping interval 'dist.step'	
VP.cumulative.distance.2D	Accumulated two-dimensional distance moved (m) between VPs, subsequent to sub-sampling according to ME, if VP.ME = TRUE and using the stepping interval 'dist.step'	

The interplay between numerical precision in R, correction rate and net error can make more than one round of adjustment necessary for dead-reckoning fixes to accord exactly with ground-truthed locations (cf. Fig. 4a), particularly given that slight discrepancies accumulate over time. Each iteration of the correction process produces a tighter adherence between estimated and ground-truthed positions [cf. 6]. Typically, this does not involve more than two rounds of VPC to achieve a maximum net error of .01 m (the threshold used within *Gundog.Tracks*) across a *ca.* (1 Hz) 2 week-long track. Logically, the net error between VPs and (corrected) dead-reckoned positions is negatively correlated with correction rate (cf. Fig. 4b) [cf. 43], although the rate of 'drop-off' is dependent on the accuracy of the initial

(uncorrected) dead-reckoned track (cf. Fig. 5), itself, modulated by the extent of system errors (Table. 1) and initial user-defined track scaling.

Within this process, people assume VPs to be perfect, however, across all VP determining methods, the rate and accuracy of data acquisition is highly moderated according to the permissiveness of the environment, such as high-density shrub or submersion in water [e.g., 35, 122, 123]. GPS technology is arguably the most popular and widely used method for determining estimates of free-ranging animal movement [cf. 124, 125, 126]. This is because inspection of data is less complex and time-consuming than some of the alternatives, whilst improvements in design and battery longevity have enabled GPS units to be attached to a plethora of animals (up to almost four orders of magnitude in size and mass [cf. 8, 127]) and record at high frequencies (e.g., ≥ 1 Hz [124, 128]). Consequently, GPS units are unparalleled for providing such detailed quantification of space-use outside of the VPC dead-reckoning framework, and are the most utilised VPC method within (including the case study datasets within this study). However, locational accuracy (excepting precision error radius [cf. 129] and variable latency [cf. 130]) can vary by a few metres or be appreciably more depending upon the propagation of signal quality and/or receiver reception capability [35, 131, 132]. As such, VP error becomes more relevant at smaller scales of assessed movement and this is the reason why VP distance-moved estimates can go from being typically underestimated at low frequencies (due to linear interpolation of tortuous movements) [23, 133, 134] to overestimated at high frequencies [91, 129] and result in highly variable correction factors within the VPC dead-reckoning process [cf. 7]. Indeed, judicious selection of VPC rate is critical in maximizing dead-reckoned track accuracy when relocation data is taken at fine spatial- and temporal resolutions [23] (cf. Table. 2 – '*VP.ME*', '*method*', '*thresh*' and '*dist.step'* inputs to

aid in modulating VPC rate). Likewise, the initial screening for location anomalies, across all VP methods and sampling intervals, is important so as to prevent incorrect distortion of tracks. Put simply, the higher the quality of VP data input, the greater the robustness of the VPC dead-reckoning output.

It was suggested by Bidder et al. [7], that the next stage in this work is to derive a standardised set of rules to maximise the value of both GPS (though this applies to any VP method) and dead-reckoned data in line with the questions being asked. We argue that consistent trends in the magnitude and/or bias of correction factors can be used as a diagnostic tool for elucidating; (i) VP inaccuracy (e.g., possibly manifested by extremely high distance and heading correction factors), (ii) required alterations to the DBA~speed relationship (e.g., due to traversing across different substrates (e.g., Fig. 5)) and (iii) drift due to current vectors [cf. 13, 43] (e.g., Fig. 6).

The case-studies

An important question to address is how often to do VP correction. This is obviously dependent upon the scales of movement elicited and the medium in/on which the animal in question navigates. Put simply, one should VP correct as little as possible, but as much as is necessary and we elaborate on this using our model species operating in different media. Within Fig. 5, the 1 Hz GPS track (blue) is plotted alongside two different dead-reckoned tracks; ((a) = uncorrected & (b) = corrected approx. every 30 mins (method = “time”)) from twelve days of data acquisition of one lion. There were two variations in the method of scaling the dead-reckoned tracks; a track based on a Vectorial Dynamic Body Acceleration (VeDBA) threshold (red), and a track advanced based on periods of identified movement (purple). The

311 *m* (multiplicative) coefficient and *c* (constant) values were determined from the VeDBA~GPS
312 speed relationship [Fig. 5, insert a_1] and the Movement Verified Filtering (MVF) protocol
313 outlined by Gunner et al. [91] was used to depict movement and anomalous GPS fixes (green)
314 and to compute reasonable GPS-derived speed estimates. This case study demonstrates three
315 important points. Firstly, on its own, dead-reckoning is subject to substantial drift and so VPC
316 is essential for resetting this error. The more frequent a user corrects, the more accurate the
317 dead reckon track becomes (relative to VPs), though VP error can also be substantial,
318 especially during rest behaviour (see Gunner et al. [91] for demonstration of this). For collared
319 animals, heading measurements can become inaccurate at times of erratic collar roll (cf.
320 Table. 1) and conjointly, GPS performance is also reduced when antenna position becomes
321 compromised [e.g., 135].
322
323 Secondly, and in conjunction to the above, irrespective of VPC rate, the initial allocation of
324 speed is important. Here, only dead-reckoning identified movement periods resulted in
325 greater accuracy than just advancing tracks based on a VeDBA threshold. This is because even
326 stationary behaviours can impart appreciable DBA [e.g., 136] (beyond the threshold), and
327 thus wrongly advance tracks. The false patterns of tortuosity created from this, whilst scaled
328 and possibly rotated with VPC (cf. Sector. 3), remain incorporated to some degree. Whilst not
329 illustrated here, advancing tracks without a VeDBA threshold would incur greater error still.
330 Lastly, in this section, the distance correction factor was consistently high [Fig. 5, insert b_1] as
331 the lion travelled along the Botswana fence boundary, perhaps as a result of the animal
332 walking on the compact dirt road at this location [Fig. 5, insert a_2], altering the VeDBA~speed
333 relationship. Such patterns in correction factors (whether consistent or highly variable) can
334 highlight issues with the underlying track scaling.

335 Where animals move in water or air, obtaining accurate estimates of speed is more difficult
336 without the use of speed sensors. Naturally, the resolution and accuracy of initial dead-
337 reckoning track scaling (pre-VPC) reduces when speed has to be approximated using constant
338 values according to behaviour type (a strategy used here). There is a balance between initial
339 dead-reckoning accuracy and required VPC. The lower the initial track accuracy, the more
340 frequent it should be corrected, and additional drift caused by external-force vectors
341 compounds this issue. Within Fig. 6, we illustrate the value that current correction, dependent
342 on current information, brings to the VPC procedure if the derived track is to be superimposed
343 on the environment. Here, one Magellanic penguin was dead-reckoned with and without tidal
344 vector integration (instantaneous tidal currents were deduced from a 3-D numerical model
345 validated in the region [137], at hourly, 1 km^2 grid nodes). Commuting speed was allocated
346 2.1 m/s [cf. 56, 138] and changed according to R_{29} (Section 3). Surface period 'rest' speed
347 were allocated 0.416 m/s [cf. 101]. VP accuracy improved considerably both pre- and post-
348 VPC when currents were integrated which points to the value of acquiring current data if
349 possible, particularly if VPs are sparse.
350
351 For all our case study animals, GPS units were set to record at 1 Hz. With this temporal
352 resolution (which is not always possible anyway due to the high-power requirements of the
353 GPS), the value of dead-reckoning would seem questionable. However, dead-reckoning can;
354 (i) work when GPS cannot – such as when an animal is underwater [e.g., 15] or in thick forest
355 [cf. 139] and it can (ii) by-pass the issues arising from GPS inaccuracies such as 'jitter' [cf. 91],
356 allowing for more accurate and finer scale delineations of movement. This is illustrated in Fig.
357 7, in which twelve outgoing (green) and incoming (blue) dead-reckoned trajectories from
358 Magellanic penguins walking to and from their nest are plotted. Incoming tracks were reverse-

359 dead-reckoned (Outgoing = FALSE, bound = FALSE), because the GPS did not always register
360 fixes for minutes after birds left the water and because nest coordinates were known [Fig. 7,
361 insert]. This explains why the blue tracks extend into the sea rather than encroach further
362 inland when speed was over-estimated. What is evident is that even 'accurate' GPS paths are
363 coarsely resolved due to precision errors. Indeed, even with little or no GPS error, this can
364 greatly compromise movement estimates [cf. 129]. Conversely, the precision of the dead-
365 reckoned tracks is only limited by the amount of initial motion sensor data under-sampling
366 (usually required in some capacity to make datasets more manageable and less
367 computationally expensive). Such fine-scale estimates can therefore (with suitable VPC) allow
368 users to define movement in space with unprecedented resolution. The benefit of this is that
369 such resolution can resolve Important metrics of movement, such as step duration [cf. 140]
370 and the number and extent of turns made [cf. 141]; useful parameters for investigating
371 navigation and foraging strategies according to environmental circumstance - though, such
372 parameters are also useful without superimposing on the environment. Moreover, even
373 dead-reckoned tracks that are sparsely corrected or never corrected can detail important
374 movement-specific behaviours [9], for example, circling behaviour [cf. 61].
375
376 Ultimately, the higher the frequency at which dead-reckoning is undertaken, the better the
377 resolution and detail of reconstructed tracks. However, accuracy only improves up to a point
378 because extrapolated travel vectors (heading and speed estimates) nearly always comprise
379 some degree of error (no matter how small) and so, with very high frequencies (> 1 Hz), more
380 error is accumulated per unit time [cf. 13, 41]. In particular, when the temporal resolution of
381 dead-reckoning results in a spatial resolution dominated more by sensor noise than by 'actual'
382 movement of the animal in question, dead-reckoning accuracy will begin to decrease (at least

pre-VPC). The extent of this will depend on the size, speed and lifestyle of the animal in question. For example, the benefits of dead-reckoning a lion at 40 Hz rather than 1 Hz are questionable (how often does a lion turn substantially within a second?), particularly given the additional computation time and possible error (relative to VPs). As such, and akin with VP under-sampling, choice of motion sensor data under-sampling is relevant to dead-reckoning accuracy, and this will be moderated according to the scales (and media) of movement elicited by the animal in question. Beyond this, Fig. 7 also demonstrates the importance of initial track advancement, with three variants used, including step counts instead of DBA.

Finally, obtaining accurate estimates of altitude or depth allow users to plot and investigate scales of continuous movement in three dimensions and at times when VP success rate fails completely (such as underwater). We demonstrate this using the Imperial cormorant in Fig. 8. After visual inspection of data, uncorrected tracks were scaled according to the following speeds: periods of flying allocated 12 m/s, surface 'rest' periods allocated 0.1 m/s, bottom phase of dives allocated 0.4 m/s and descent and ascent speeds modulated according to E_{14} (Section 3). Note that elevation was not resolved during flying periods (although flying periods were dead-reckoned). Regardless of the current limitations, the VPC dead-reckoning procedure represents a substantial advance for resolving, and thereby allowing investigation of, continuous, fine-scale, free-ranging 2- or 3-D space use with all its underlying scales of tortuosity and distances moved (e.g., Fig. 7 & 8).

3. VPC dead-reckoning procedure in R

We provide complementary scripts and further expand on key concepts in the supplementary information, referred to in the text as 'SI_x', and refer to mathematical equations as 'E_x' and R syntax as 'R_x', where 'x' is the reference number. To simplify concepts, we use base R syntax (wherever possible) and typically use vectors to demonstrate points made, though 'df$' directly before the variable name indexes data retained within data frame columns (assuming data frame is called 'df'). We note, however, that more efficient code implementations are possible (e.g., *data.table* [142] and lapply()) than presented here, especially for large data, but wanted to make the code as readable as possible in this manuscript, especially to persons not familiar with complex coding. More efficient code will be implemented through updated GitHub versions of the functions. See SI_1 for our model species' device set up and capture protocol.

<u>The order and content of SIs are listed below:</u>

SI_1 – Methods expanded (.doc)

- Device set up and capture protocol

SI_2– Ensuring the correct coordinate system axis alignment (.doc)

- Orthogonal set up with respect to the North-East-Down (NED) local frame
- Transforming between coordinate frames
- Configuration calibration to aid axis alignment

SI_3 - Magnetometer calibration and deriving yaw (.doc)

- Calibration period required to correct the magnetic distortions
- Soft and hard iron distortions
- *Gundog.Compass()* (.R file)

SI_4- Step counts as a distance estimate (.doc)

- *Gundog.Peaks()* (.R file)

SI_5- Time data in R (POSIXct) (.doc)

- Creating POSIXct timestamp object
- Converting between time formats
- Decimal seconds
- Examples of manipulating time data

SI_6 - VPC dead-reckoning (.doc)

- *Gundog.Tracks()* (.R file)

SI_7 – Step by step guide of using *Gundog.Tracks* (.R file) (to use in conjunction with below)

- Raw sensor and GPS data frame (.txt) of a penguin walking out to sea from its nest

3.1 Preparing the three axes of rotation for derivation of heading

The tilt-compensated compass method is a well-known practice for deriving heading [e.g., 18, 19, 76]. Correct coordinate system axis alignment and suitable calibration of tri-axial magnetometry data [cf. 143] are crucial pre-processors, without which, heading estimates would likely incorporate substantial error [cf. 18, 143]. The tilt-compensated compass method described below (following the framework outlined by Pedley [18]), requires the aerospace (x-North, y-East, z-Down) coordinate system, or 'NED' (cf. SI_2: Fig. 1). We provide examples of axis alignment, outline the importance of transforming between coordinate frames and recommend a universal configuration calibration procedure to aid correct axis alignment within SI_2.

Multiple mathematically sophisticated algorithms have been developed to correct distortions from each magnetometer channel's output [e.g., 20, 143, 144, 145, 146]. We provide an annotated R script - *Gundog.Compass* (SI_3) that corrects both soft and hard iron distortions from tri-axial magnetometry data and subsequently computes tilt-compensated heading (0^o to 360^o). Within this function, there are two main methods of correction to choose from, based on the mathematical protocols outlined by Vitali [147] - least-square error

approximation (constructing an ellipsoid rotation matrix) and Winer [148] - scale biases with simple orthogonal rescaling (avoiding matrices altogether). We expand on this user-defined functionality, as well as outlining the causes of soft and hard iron distortions and the initial calibration procedure required to correct such distortions, including within SI_3.

Tilt-compensated heading derivation

For the correct computation of heading, two of the magnetometer channels need to align parallel to the earth's surface. This is achieved by correcting any orientation (de-rotation) according to pitch and roll angles (postural offsets). These angles are typically approximated by deriving gravity-based (static) acceleration [see 67, 149] from each channel by employing one of four approaches using; (i) a running mean [e.g., 67, 81], (ii) a Fast-Fourier transformation [e.g., 150], (iii) a high-pass filter [e.g., 151] or (iv) a Kalman-filter [e.g., 152]. Here, we use a computationally simple running mean over 2 seconds [67] (E_1).

$$G_{x,y,z} = \frac{1}{w} \sum_{j=i-\frac{w}{2}}^{i+\frac{w}{2}} A_{x,y,z} \qquad (E_1)$$

Where, *w* is an integer specifying the window size and $G_{x,y,z}$ and $A_{x,y,z}$ represents the smoothed and raw components of acceleration, respectively. In the absence of linear (dynamic) acceleration [see 149, 153], values of $G_{x,y,z}$ reflect the device orientation with respect to the earth's reference frame (though see Table. 1).

In R, the '*zoo*' package [119] provides useful wrappers to apply arithmetic operations in a rolling fashion ($R_{1:4}$).

```
install.packages("zoo") ; library(zoo)                                    (R1)


Gx = rollapply(Ax, width=w, FUN=mean, align="center", fill="extend")       (R2)
Gy = rollapply(Ay, width=w, FUN=mean, align="center", fill="extend")       (R3)
Gz = rollapply(Az, width=w, FUN=mean, align="center", fill="extend")       (R4)
```

Here, *w* should be replaced with the window width of choice (e.g., for 20 Hz data and a smoothing of 2 seconds required, replace *w* with 40). We use a centre-aligned index (compared to the rolling window of observations), with "extend" to indicate repetition of the leftmost or rightmost non-NA value (though fill can equally be set as NA, 0, etc.).

Importantly, for correct trigonometric formulae output within the tilt-compensated compass method, the vectorial sum of static acceleration ($G_{x,y,z}$) and calibrated magnetometry ($M_{x,y,z}$) measurements across all three spatial-dimensions must be normalised with a scaled magnitude (radius) of one ($E_{2:3}$, $R_{5:10}$). Prior to this normalisation process, it may be of value to initially smooth out small deviations within magnetometry data (e.g., due to anomalous spikes in magnetic inference) (see E_1, $R_{1:R4}$). We used a smoothing window of 10 events for the 40 Hz datasets used in this study.

$$\begin{bmatrix} NG_x \\ NG_y \\ NG_z \end{bmatrix} = \frac{1}{\sqrt{G_x \bullet G_x \bullet G_y \bullet G_y \bullet G_z \bullet G_z}} \bullet \begin{bmatrix} G_x \\ G_y \\ G_z \end{bmatrix} \quad (E_2) \quad \begin{bmatrix} NM_x \\ NM_y \\ NM_z \end{bmatrix} = \frac{1}{\sqrt{M_x \bullet M_x \bullet M_y \bullet M_y \bullet M_z \bullet M_z}} \bullet \begin{bmatrix} M_x \\ M_y \\ M_z \end{bmatrix} \quad (E_3)$$

```
NGx = Gx / sqrt(Gx^2 + Gy^2 + Gz^2)                                       (R5)
NGy = Gy / sqrt(Gx^2 + Gy^2 + Gz^2)                                       (R6)
NGz = Gz / sqrt(Gx^2 + Gy^2 + Gz^2)                                       (R7)

NMx = Mx / sqrt(Mx^2 + My^2 + Mz^2)                                       (R8)
NMy = My / sqrt(Mx^2 + My^2 + Mz^2)                                       (R9)
NMz = Mz / sqrt(Mx^2 + My^2 + Mz^2)                                       (R10)
```

Pitch (θ) and roll (Φ) are calculated using rotation matrices and because there are multiple variations in the order that these can be composed and applied, there are also variant (valid) equations that output different pitch and roll angle estimates, for equivalent static acceleration input. The convention is to use formulae that restrict either the pitch or the roll angles within the range -90° to +90° (but not both), with the other axis of rotation able to lie between -180° and 180° (see $E_{4:5}$). The aerospace sequence typically allows roll angles to have the greater freedom and this is relevant for studies using collar-mounted tags, whereby collar may roll > 90° in either direction from default orientation.

$$\theta = atan2\left(-NG_x, \sqrt{\left(NG_y \bullet NG_y + NG_z \bullet NG_z\right)}\right) \bullet \frac{180}{\pi} \quad (E_4)$$

$$\Phi = atan2\left(NG_y, NG_z\right) \bullet \frac{180}{\pi} \quad (E_5)$$

The equation for roll (E_5) however, has a region of instability at obtuse pitch angles (e.g., for NED systems, the x-axis points directly up or down, with respect to the Earth's frame of reference). Whilst there is no 'gold standard' solution to this problem of singularity (using Euler angles), an attractive circumvention (detailed within [153]) is to modify (E_5) and add a very small percentage (μ) of the GN_x reading into the denominator, preventing it ever being zero and thus driving roll angles to zero when pitch approaches -/+ 90° for stability (E_6).

$$\Phi = atan2\left(NG_y, sign(NG_z) \bullet \sqrt{(NG_z \bullet NG_z + \mu \bullet NG_x \bullet NG_x)}\right) \bullet \frac{180}{\pi} \quad (E_6)$$

Where, $sign(NG_z)$ is allocated the value +1 when NG_z is non-negative and -1, when NG_z is negative (recovers directionality of NG_z, subsequent to the square-root).

Taken together then, in R, pitch and roll are computed according to, ($R_{11:13}$) with outputs within the range of -90° to +90° for pitch and -180° to +180° for roll, and this is the formula we use in the tilt compensated method outlined below (and within SI_3).

```
mu = 0.01 ; sign = ifelse(NGz >= 0, 1, -1)                    (R11)
Pitch = atan2(-NGx, sqrt(NGy^2 + NGz^2)) * 180/pi             (R12)
Roll = atan2(NGy, sign * sqrt(NGz^2 + mu * NGx^2)) * 180/pi   (R13)
```

Here, prior to the derivation of pitch and roll, μ is allocated the value 0.01 (R_{11}) and a vector termed '*sign*' is created, containing 1's and -1's according to the direction of measured *g* from NG_z (R_{12}). Note, standard trigonometric functions operate in radians, not degrees. In base R, π = pi. Multiplying values by *pi*/180 coverts degrees into radians, whilst multiplying values by 180/*pi* does the reverse.

A device is de-rotated by multiplying by the inverse roll and then the inverse pitch rotation matrices, which when expanded out gives (E_7).

$$\begin{bmatrix} NMf_x \\ NMf_y \\ NMf_z \end{bmatrix} = \begin{bmatrix} NM_x \bullet \cos(\theta) + NM_y \bullet \sin(\theta) \bullet \sin(\Phi) + NM_z \bullet \sin(\theta) \bullet \cos(\Phi) \\ NM_y \bullet \cos(\Phi) - NM_z \bullet \sin(\Phi) \\ -NM_x \bullet \sin(\theta) + NM_y \bullet \cos(\theta) \bullet \sin(\Phi) + NM_z \bullet \cos(\theta) \bullet \cos(\Phi) \end{bmatrix} \quad (E_7)$$

Here, $NMf_{x,y,z}$ are the calibrated, normalised magnetometry data after tilt-correction. Finally, yaw (ψ) (heading) can be computed from the NMf_x and NMf_y (E_8) *via;*

$$\psi = atan2(-NMf_x, NMf_x) \bullet \frac{180}{\pi} \quad (E_8)$$

We outline the R code for this procedure below ($R_{14:22}$).

```
RollSinAngle = sin(Roll * pi/180)     (R14)
RollCosAngle = cos(Roll * pi/180)     (R15)
PitchSinAngle = sin(Pitch * pi/180)   (R16)
```

```
PitchCosAngle = cos(Pitch * pi/180)                                          (R17)
NMfx = NMx * PitchCosAngle + NMy * PitchSinAngle * RollSinAngle +            (R18)
NMz * PitchSinAngle * RollCosAngle
NMfy = NMy * RollCosAngle - NMz * RollSinAngle                               (R19)
NMfz = -NMx * PitchSinAngle + NMy * PitchCosAngle * RollSinAngle +           (R20)
NMz * PitchCosAngle * RollCosAngle
Yaw = atan2(-NMfy, NMfx) * 180/pi                                            (R21)
Yaw = ifelse(Yaw < 0, Yaw + 360, Yaw)                                        (R22)
```

Note, yaw output from (R_{21}) uses the scale -180° to + 180°. (R_{22}) converts to the scale 0° to 360° (specifically, 0° to 359.9°). This is also achieved by using a modulus (mod) operator (E_9, R_{23}), which in base R takes the form *%%*.

$$\psi = mod(360 + \psi, 360) \quad (E_9)$$

```
Yaw = (360 + Yaw) %% 360                                                     (R23)
```

Magnetic declination is defined as the angle on the horizontal plane between magnetic north and true north [154]. Prior to dead-reckoning, magnetic declination should be summed to heading values to convert from magnetic to true North [155]. There are many online sources to calculate the magnetic declination of an area [e.g., 156]. Notably, logical corrections may need to be performed to ensure data does not exceed either circular direction after applying magnetic declination (R_{24}).

```
h = ifelse(h < 0, h + 360, h) ; h = ifelse(h > 360, h - 360, h)              (R24)
```

where *h* refers to the vector containing the heading data.

3.2 Preparing speed estimates

The vectorial dynamic body acceleration (VeDBA) (E_{10}) [cf. 62, 157] was our choice of DBA-based speed proxy for terrestrial dead-reckoning purposes. This is given by;

$$v = \sqrt{({D_x}^2 + {D_y}^2 + {D_z}^2)} \quad (E_{10})$$

Where v represents VeDBA, D_x, D_y & D_z are the dynamic acceleration values from each axis, themselves obtained by subtracting each axis' static component of acceleration (cf. E_1, $R_{1:4}$) from their raw equivalent (R_{25}).

```
v = sqrt((Ax - Gx)^2 + (Ay - Gy)^2 + (Az - Gz)^2)
```
(R_{25})

Where, *Ax, Ay, Az* and *Gx, Gy, Gz* are the raw and static (smoothed) values of each channel's recorded acceleration.

We recommend implementing a running mean (cf. E_1, $R_{1:4}$) to raw VeDBA values to ensure that both acceleration and deceleration components of a stride cycle are incorporated together per unit time and to reduce the magnitude of small temporal spikes, (likely not attributable to the scale of movement elicited [cf. 91]. Choice of smoothing window size is dependent on the scale of movement being investigated, though as a basic rule, we suggest 1 to 2 seconds. For similar reasons, it is also worth post-smoothing raw pitch, roll and heading outputs, although heading requires a circular mean ($E_{11:12}$) [cf. 158].

$$\bar{\theta}_p = atan2\left(\frac{1}{n}\sum_{j=i}^{n}\sin(h_j \bullet \frac{\pi}{180}),\ \frac{1}{n}\sum_{j=i}^{n}\cos(h_j \bullet \frac{\pi}{180})\right) \quad (E_{11})$$

$$\bar{h} = mod\left(360 + \left(\bar{\theta}_p \bullet \frac{180}{\pi}\right), 360\right), \quad (E_{12})$$

where h_j and $\bar{h}$ are the unsmoothed and smoothed heading values, $\bar{\theta}_p$ the arithmetic mean after converting degrees to cartesian coordinates and mod refers to the modulo operator.

In R, the above formula can be made into a function (R_{26}), to be applied within the '*rollapply*' wrapper (replacing 'FUN = *mean*' with 'FUN = *Circ.Avg*') (cf. $R_{1:4}$).

```
Circ.Avg = function(x){                                          (R26)
H.East = mean(sin(x * pi / 180))
H.North = mean(cos(x * pi / 180))
MH = (atan2(H.East, H.North)) * 180/pi
MH = (360 + MH) %% 360
return(MH)
}
```

Speed (s) can be estimated from VeDBA (v) *via* (E_{13}).

$$s = (v \bullet m) + c \qquad (E_{13})$$

Where m is the coefficient of proportionality and c is a constant [7, 64]. Here, a user can define various bouts of movement from motion sensor data (e.g., *via* various machine learning approaches (for review see Farrahi et al. [159]) or the Boolean-based LoCoD method [95]) and/or substrate condition (e.g., *via* GPS), to be cross-referenced when allocating variants of the speed coefficients. As a simple example, in R, should walking (coded for as 1) and running (coded for as 2) be teased apart from all other (non-moving) data (coded for as 0) within a Marked Events vector (*ME*), then *ME* can be used to allocate various m (and if applicable, c) values using simple 'ifelse' statements ($R_{27:28}$).

```
m = ifelse(ME == 1, 1.5, ifelse(ME == 2, 3.5, 0))                (R27)
c = ifelse(ME > 0, 0.1, 0)                                       (R28)
```

Here, walking is given an arbitrary coefficient of 1.5 and running, 3.5 with a value of 0.1 for their constants. All other *ME* values are given a 0 coefficient and 0 constant, which results in no speed at such times, regardless of DBA magnitude.

By-passing DBA as a speed proxy

Dividing the number of steps detected within a given rolling window length (cf. $R_{1:4}$), by the window length (s) gives an estimated step count per second. This can be converted to speed by multiplying by a distance per step estimate (assuming constant distance travelled between step gaits). We review this further in SI_4, including a simple peak finder function – *Gundog.Peaks* that locates peaks based on local signal maxima, using a given rolling window, with each candidate peak filtered according to whether it surpassed a threshold height (in conjunction with other potential user-defined thresholds). Note, this method can equally be applied to non-terrestrial species, using flipper/tail beats instead, where appropriate.

For diving animals, a proxy for horizontal speed can be obtained based on animal pitch and rate change in depth [44, 109]. Specifically, rate change of depth (Δd) (units in m/s) is divided by the tangent of pitch (θ) (converted from degrees to radians) (E_{14}).

$$s = \frac{\Delta d}{\tan\left(\theta \bullet \frac{\pi}{180}\right)} \qquad (E_{14})$$

Here, resultant speed values need to be made absolute (positive). This calculation is only valid when the direction of movement is the same as the direction of the animal's longitudinal axis (equal pitch assumption) [cf. 44] and thus should only be calculated at times when the animal is travelling 'ballistically' (at considerable vertical speed). An upper limit should be imposed on speed values derived in this way because values can become highly inflated when the pitch angle is particularly acute.

```
s = ifelse(abs(p) >= 10, abs(RCD / tan(p * pi/180)), s)          (R29)
```

In the above example (R_{29}), nominal speed values are overwritten with the trigonometric formula output (E_{14}) at times of 'appreciable' pitch (10^{o}) [cf. 160], where *RCD* is the rate change of depth and *p* is the pitch (in radians).

3.3 Converting speed to a distance coefficient

Speed (s) estimates are multiplied by the time difference between the values (TD) to give a distance estimate (units in metres) which, in turn, standardises coefficient comparisons across datasets sampled at different rates. These distance values are then divided by the approximate radius of the earth (*R* = 6378137 m) to give a radial distance coefficient (q) [see 161] (E_{15}).

$$q = \frac{s \bullet TD}{R} \qquad (E_{15})$$

Assuming that high resolution depth data is not available, but 'absolute' speed estimates have been obtained, then an alternative to E_{14}, (in accordance with the equal pitch assumption) is to derive horizontal distance estimates by multiplying the absolute distance by the cosine of the pitch (θ) (converted from degrees to radians), which can equally be performed on the radial distance (E_{16}).

$$q = q \bullet \cos\left(\theta \bullet \frac{\pi}{180}\right) \qquad (E_{16})$$

In R, to determine accurate lengths of time between values, it is best to save date and time variables together as *POSIX* class [162]. Creating timestamp (TS) objects with *POSIXct* class enables greater control and manipulation of time data. This makes computing the rolling time difference (TD) (units in seconds) between data points simple (R_{30})

```r
TD = c(0, difftime(TS, lag(TS), units = "secs")[-1])
```
(R_{30})

We detail how to create timestamp objects of *POSIXct* class within SI_5, including formatting with decimal seconds (important for infra-second datasets) and various codes useful for manipulating data to be dead-reckoned based on time.

In R then, following the computation of TD, q is obtained *via* ($R_{31:32}$).

```r
s = (v * m) + c
```
(R_{31})

```r
q = (s * TD) / 6378137
```
(R_{32})

Note, if a negative *c* intercept is used (e.g., to allow for some body movement without translation), then any negative speed values would need to be equated to zero as an additional step.

As previously mentioned, the *ME* vector (progressive movement coded by integer values greater than zero (e.g., 1) and stationary behaviour coded by zero) can be used to ensure *q* (essentially the distance moved) is zero when *ME* reads zero, ensuring dead-reckoned tracks are not advanced at such times, regardless of the computed speed (R_{33}).

```r
q = ifelse(ME == 0, 0, q)
```
(R_{33})

3.4 Derivation of co-ordinates

Once q and h are obtained, coordinates are advanced using ($E_{17:18}$);

$$Lat_i = \operatorname{asin}(\sin Lat_0 \bullet \cos q + \cos Lat_0 \bullet \sin q \bullet \cos h) \quad (E_{17})$$

$$Lon_i = Lon_0 + \operatorname{atan2}\big((\sin h \bullet \sin q \bullet \cos Lat_0), (\cos q - \sin Lat_0 \bullet \sin Lat_i)\big) \quad (E_{18})$$

Where Lat_0, Lat_i and Lon_0, Lon_i are the previous and present latitude and longitude coordinates, respectively, h is the (present) heading in radians and q is the (present) distance coefficient.

In R, the above can be performed iteratively within a for-loop (iteration of code repeated per consecutive i_{th} element of data) (R_{37}). Initializing the output latitude (*DR.lat*) and longitude (*DR.lon*) variables to the required length (e.g., as governed by the vector length of other input data (heading, speed, etc.) speeds up processing time (R_{34}). Within the trigonometric dead-reckoning formulae, the starting latitude (*la*) and longitude (*lo*) coordinates and heading (h) values must be supplied in radians (R_{35}). The *la* and *lo* values are saved as the first elements of the *DR.lat* and *DR.lon* vectors to be advanced, respectively (R_{36}).

```
DR.lat = rep(NA, length(h)) ; DR.lon = rep(NA, length(h))                    (R34)
la = la * pi/180 ; lo = lo * pi/180 ; h = h * pi/180                         (R35)
DR.lat[1] = la DR.lon[1] = lo                                                (R36)

for(i in 2:length(DR.lat)) {                                                 (R37)
      DR.lat[i] = asin(sin(DR.lat[i-1]) * cos(q[i]) + cos(DR.lat[i-1]) *
      sin(q[i]) * cos(h[i]))
      DR.lon[i] = DR.lon[i-1] + atan2(sin(h[i]) * sin(q[i]) *
      cos(DR.lat[i-1]), cos(q[i]) - sin(DR.lat[i-1]) * sin(DR.lat[i]))
}
```

Reverse dead-reckoning

For this, firstly, the time difference is computed as usual (R_{38}) and the dimensions of each vector required in the dead-reckoning calculation are reversed. We bind all relevant vectors into a data frame (df) (R_{39}), subsequent to reversing data frame dimensions (R_{40}); the last row becomes the first row, second to last row becomes the second etc. Note, this can equally be achieved by using the *rev()* function within base R, on each individual vector. These reversed columns are now restored as vectors (R_{41}) and shifted forward by one element (R_{42}) (required

for correct alignment in time so that dead-reckoning works in exactly the opposite manner to 'forward' dead-reckoning).

```
TD = c(0, difftime(TS, lag(TS), units = "secs")[-1])                    (R38)
df = data.frame(TD, h, v, m, c, ME)                                     (R39)
df = df[dim(df)[1]:1, ]                                                 (R40)
TD = df[, 'TD'] ; h = df[, 'h']  ; v = df[, 'v'] ;                      (R41)
m = df[, 'm'] ; c = df[, 'c'] ; ME = df[, 'ME']
TD = c(NA, TD[-length(TD)]) ; h = c(NA, h[-length(h)]) ;                (R42)
v = c(NA, v[-length(v)]) ; m = c(NA, m[- length(m)]) ;
c = c(NA, c[-length(c)]) ; ME = c(NA, ME[-length(ME)])
```

The next step is to rotate heading 180° and correct for its circular nature (R_{43}).

```
h = h - 180 ; h = ifelse(h < 0, h + 360, h)                             (R43)
```

Lastly, *q* is determined and *DR.lon* and *DR.lat* are advanced based on the dead-reckoning formula (cf. $R_{34:37}$), except in this instance, the first element of *DR.lon* and *DR.lat* needs to be supplied by the 'known' last *lo* and *la* coordinates.

Integrating current vectors

In R, current vectors can be added according to ($R_{44:48}$). Current strength (*cs*) is in m/s (ensure values are absolute) and current heading (*ch*) uses the scale 0° to 360°. Note the use of '*yy*' and '*xx*' vectors, storing the previous *DR.lat* and *DR.lon* coordinates prior to implementing the next 'current drift' vector per iteration. The current strength is also standardised according to the time period length and Earth's radius (analogous to the derivation of *q*). When reverse dead-reckoning, it is important to ensure that *cs* and *ch* are included in the steps outlined above ($R_{38:43}$).

```
DR.lat = rep(NA, length(h)) ; DR.lon = rep(NA, length(h))               (R44)
xx <- rep(NA, length(cs)) ; yy <- rep(NA, length(cs))                   (R45)
la = la * pi/180 ; lo = lo * pi/180 ;                                   (R46)
```

```
h = h * pi/180 ; ch = ch * pi/180
DR.lat[1] = la DR.lon[1] = lo                                    (R47)
for(i in 2:length(DR.lat)) {                                     (R48)

      DR.lat[i] = asin(sin(DR.lat[i-1]) * cos(q[i]) + cos(DR.lat[i-1]) *
      sin(q[i]) * cos(h[i]))
      yy[i] = DR.lat[i]
      DR.lon[i] = DR.lon[i-1] + atan2(sin(h[i]) * sin(q[i]) *
      cos(DR.lat[i-1]), cos(q[i]) - sin(DR.lat[i-1]) * sin(DR.lat[i]))
      xx[i] = DR.lon[i]
      DR.lat[i] = asin(sin(yy[i]) * cos((cs[i] * TD[i]) / 6378137) +
      cos(yy[i]) * sin((cs[i] * TD[i]) / 6378137) * cos(ch[i]))
      DR.lon[i] = xx[i] + atan2(sin(ch[i]) * sin((cs[i] * TD[i]) /
      6378137) * cos(yy[i]), cos((cs[i] * TD[i]) / 6378137) - sin(yy[i]) *
      sin(DR.lat[i]))

}
```

3.4 VPC procedure

Specifically, this method entails calculating the difference of Haversine distance (net error) and bearing (from true North) between consecutive VPs and the corresponding time-matched dead-reckoned track positions. The trigonometric Haversine formulae ($E_{19:20}$) are used to calculate the great-circle distance (d) and great circular bearing (b) between consecutive VPs and consecutive (time-matched) dead-reckoned positions (note we use the term 'bearing' to differentiate between heading estimates from motion data – though they are essentially the same).

$$d = 2 \bullet R \bullet sin^{-1}\left(\sqrt{sin^2\left(\frac{Lat_i - Lat_0}{2}\right) + \cos(Lat_0) \bullet \cos(Lat_i) \bullet sin^2\left(\frac{Lon_i - Lon_0}{2}\right)}\right) \quad (E_{19})$$

Where, R is the Earth's radius and d, the output in metres.

$$\mathrm{b} = atan2\begin{pmatrix} sin(\Delta Lon) \bullet cos(Lat_i), \\ cos(Lat_0) \bullet sin(\Delta Lat) \bullet cos(Lat_i) \bullet cos(\Delta Lon) \end{pmatrix} \bullet \frac{180}{\pi} \quad (E_{20})$$

where, ΔLon represents Lon_i - Lon_0, ΔLat represents Lat_i - Lat_0 and b output is in the scale -180 º to +180º. To convert b to the conventional 0º to 360º scale, 360 should be added to values < 0.

For each VP, the distance is divided by the dead-reckoned distance providing a distance correction factor (ratio) (E_{21}). The heading correction factor is computed by subtracting the dead-reckoned bearing from the VP bearing (E_{22}). To ensure that difference does not exceed 180º in either circular direction, 360 should be added to values < -180 and 360 subtracted from values > 180. A simple example of why this is relevant can be illustrated by subtracting a dead-reckoned bearing value of 359º from a VP bearing value of 1º – post correction, the difference is +2º.

$$Distance_{corr.factor} = \frac{Distance_{VP}}{Distance_{DR}} \quad (E_{21})$$

$$Heading_{corr.factor} = Bearing_{VP} - Bearing_{DR} \quad (E_{22})$$

All intermediate q values are multiplied by the distance correction factor and the heading correction factor is added to all intermediate h values (ensuring that h values are in degrees). To ensure circular range is maintained between 0º and 360º, 360 should be subtracted from values > 360 and added to values < 0.

Specifically, we follow the protocol illustrated within Figure 9 for intermediate values. Note the formulae to calculate both distance (d) (E_{19}) and bearing (b) (E_{20}) between two points, are also used to recalculate both the heading (h) and radial distance (q) between current-integrated dead-reckoned fixes (pre-VPC) (cf. R_{48}).

In R, the formulae to calculate the great-circle distance and great circular bearing are saved within the *disty* (R_{49}) and *beary* (R_{50}) functions, respectively, where *lon1, lat1, long2* and *lat2*

represent longitude and latitude positions (decimal format) at t_i and t_{i+1}, (t representing time).

```
disty = function(long1, lat1, long2, lat2) {                              (R49)

      long1 = long1 * pi/180 ; long2 = long2 * pi/180 ; lat1 = lat1 *
      pi/180 ;  lat2 = lat2 * pi/180
      a = sin((lat2 - lat1) / 2) * sin((lat2 - lat1) / 2) + cos(lat1) *
      cos(lat2) * sin((long2 - long1) / 2) * sin((long2 - long1) / 2)
      c = 2 * atan2(sqrt(a), sqrt(1 - a))
      d = 6378137 * c
      return(d)
}

beary = function(long1, lat1, long2, lat2) {                              (R50)

      long1 = long1 * pi/180 ; long2 = long2 * pi/180 ; lat1 = lat1 * pi/1
      80 ;  lat2 = lat2 * pi/180
      a = sin(long2 - long1)*cos(lat2)
      b = cos(lat1) * sin(lat2) - sin(lat1) * cos(lat2) * cos(long2 - long
      1)
      c = ((atan2(a, b) / pi)*180)
      return(c)
 }
```

Below, we outline an example of VPC in R and assume VP coordinates (decimal format) are aligned in the same length vectors/columns as motion sensor-derived data, e.g., heading, DBA/speed etc, with the corresponding indexed (element-/row-wise) time. Typically, motion sensor data is recorded at much higher frequency so that there are many dead-reckoned fixes between sequential VPs. As such, in the example below, we assume NA's are expressed in the VP longitude and latitude fields at times of missing locational data. This approach of synchronising VP- with motion sensor data also applies when integrating current data; assuming *ch* and *cs* are element/row-wise matched to the relevant VP grid node.

Firstly, an indexing row number (*Row.number*) vector, the length of the data used in the dead-reckoning operation (e.g., h) is created (R_{51}), which is relevant for merging full-sized and under-sampled data frames together (seen later). Together, the row number, (un-corrected) dead-reckoned longitude and latitude coordinates, VP longitude and latitude coordinates, heading and the radial distance vectors are inputted column-wise into a 'main' data frame, termed '*df*' (R_{52}) (user-assigned column names of each vector are within quotation marks). This data frame is then filtered removing rows with missing VP data and stored as *df.sub* (R_{53}). This under-sampled data frame thus, row-wise, contains the time-matched dead-reckoned and ground-truthed positions. The VPC process is analogous for reverse dead-reckoned tracks – although *VP.lon* and *VP.lat* must also be reversed (*Row.number* remains in ascending order (not reversed)). The first element of *VP.lon* and *VP.lat* must be the *lo* and *la*, respectively (or for reverse dead-reckoning, the last element prior to reversing these vectors).

```
Row.number = rep(1:length(h))                                          (R51)
df = data.frame(Row.number, 'DR.longitude' = DR.lon,                   (R52)
  'DR.latitude' = DR.lat, 'VP.longitude' = VP.lon,
  'VP.latitude' = VP.lat, h, q)
df.sub = df[!with(df, is.na(VP.longitude) | is.na(VP.latitude)) ,]     (R53)
```

Both sets of dead-reckoned and VP coordinates are shifted backwards one row within new columns termed; *DR.loni, DR.lati, VP.loni, VP.lati* (R_{54}). Row-wise, these columns represent the consecutive fix at t_{i+1} with their originals being t_i. This provides the correct format for the inputs required within the *disty* (cf. R_{49}) and *beary* (cf. R_{50}) functions. The distances between consecutive dead-reckoned estimates are stored within the column termed *DR.distance* (R_{55}) and the corresponding distances between VPs are stored within the column termed *VP.distance* (R_{56}). The *VP.distance* is divided by the *DR.distance* to provide the

distance correction factor, termed *Dist.corr.factor* (R_{57}). Importantly here, an ifelse statement is incorporated so that *Dist.corr.factor* defaults to zero at times when both *VP.distance* and *DR.distance* are zero (otherwise dividing zero by zero in R produces *NaN's*).

```
df.sub$DR.loni = c(df.sub[-1, 'DR.longitude'], NA)                    (R54)
df.sub$DR.lati = c(df.sub[-1, 'DR.latitude'], NA)
df.sub$VP.loni = c(df.sub[-1, 'VP.longitude'], NA)
df.sub$VP.lati = c(df.sub[-1, 'VP.latitude'], NA)
df.sub$DR.distance= disty(df.sub$DR.longitude,                        (R55)
df.sub$DR.latitude, df.sub$DR.loni, df.sub$DR.lati)
df.sub$VP.distance= disty(df.sub$VP.longitude,                        (R56)
df.sub$VP.latitude, df.sub$VP.loni, df.sub$VP.lati)
df.sub$Dist.corr.factor = ifelse(df.sub$VP.distance == 0 &            (R57)
df.sub$DR.distance == 0, 0, df.sub$VP.distance / df.sub$DR.distance)
```

Analogous to the distance correction, the bearings between consecutive dead-reckoned estimates are stored within the column termed *DR.head* (R_{58}) and the corresponding bearings between VPs are stored within the column termed *VP.head* (R_{59}). Logical corrections are performed to convert both to the 0° to 360° scale (R_{60}), *DR.head* is subtracted from *VP.head* providing the heading correction factor, termed *Head.corr.factor* (R_{61}) and further logical corrections are performed to ensure a minimum and maximum difference range between -180° to +180° (R_{62}).

```
df.sub$DR.head = beary(df.sub$DR.longitude,                           (R58)
df.sub$DR.latitude, df.sub$DR.loni, df.sub$DR.lati)
df.sub$VP.head = beary(df.sub$VP.longitude,                           (R59)
df.sub$VP.latitude, df.sub$VP.loni, df.sub$VP.lati)
df.sub$DR.head = ifelse(df.sub$DR.head < 0,                           (R60)
df.sub$DR.head + 360, df.sub$DR.head)
df.sub$VP.head = ifelse(df.sub$VP.head < 0,
df.sub$VP.head + 360, df.sub$VP.head)
df.sub$Head.corr.factor = df.sub$VP.head - df.sub$DR.head             (R61)
df.sub$Head.corr.factor = ifelse(df.sub$Head.corr.factor < -180,      (R62)
(df.sub$Head.corr.factor + 360), df.sub$Head.corr.factor)
df.sub$Head.corr.factor = ifelse(df.sub$Head.corr.factor > 180,
(df.sub$Head.corr.factor - 360), df.sub$Head.corr.factor)
```

Only the relevant columns; *Row.number, Dist.corr.factor* and *Head.corr.factor* are preserved (R_{63}) and merged back into the main data frame (*df*) based on the matching row numbers (R_{64}). Both *Dist.corr.factor* and *Head.corr.factor* express NA's between VPs. These are replaced with the most recent non-NA (observations carried forwards) (R_{65}). *Dist.corr.factor* and *Head.corr.factor* values are shifted forward by one row (R_{66}) for correct alignment purposes with respect to h and q values to be adjusted (cf. Fig. 9) ($R_{67:68}$). A logical correction is performed to ensure that a 0° to 360° circular scale is maintained after the heading correction (R_{69}). Note, the *na.locf()* function is required from the '*zoo*' package, to replace NA values with the last non-NA value.

```
                                                                    (R63)
df.sub = df.sub[, c('Row.number', 'Dist.corr.factor', 'Head.corr.factor')]

                                                                    (R64)
df = merge(df, df.sub, by = "Row.number", all = TRUE)

df$Dist.corr.factor = na.locf(df$Dist.corr.factor)                  (R65)
df$Head.corr.factor = na.locf(df$Head.corr.factor)
df$Dist.corr.factor = c(NA, df$Dist.corr.factor[-nrow(df)])         (R66)

df$Head.corr.factor = c(NA, df$Head.corr.factor[-nrow(df)])

q = (df$q * df$Dist.corr.factor)                                    (R67)
h = (df$h + df$Head.corr.factor)                                    (R68)
h = ifelse(h > 360, h - 360, h) ; h = ifelse(h < 0, h + 360, h)     (R69)
```

These updated coefficients are substituted into the dead-reckoning formula (cf. $R_{34:37}$) and this process is repeated iteratively (using the updated dead-reckoned coordinates, heading and radial distance each time) until dead-reckoning fixes accord 'exactly' (*Gundog.Tracks* uses a threshold of .01 m) with ground-truthed locations. An important pitfall of the correction process to consider is that dividing a value > 0 by 0 results in infinite (*Inf*) values in R. This can arise during the correction process when there is a given distance between consecutive VPs,

but no displacement between the according dead-reckoned positions. This can be a consequence of ground-truthing too frequently (typically relevant to high-res GPS studies), where positional noise is more apparent during rest periods [cf. 91] and/or wrongly assigned speed estimates/*ME* values. *Gundog.Tracks* automatically resamples VPC rate when necessary to avoid *Inf* values, essentially by ensuring that the dead reckoned track has advanced between consecutive VPs. Lastly, *Gundog.Tracks* outputs messages to the user's console, detailing up to six stages of dead-reckoning progression, which includes reporting the maximum distance (units in metres) between dead-reckoned- and ground-truthed positions (used within the VPC procedure) at each iteration of correction and whether automatic VPC resampling due to *Inf* values occurred.

4. Conclusion

We have provided a comprehensive, fully integrated application of the dead-reckoning procedure within the framework of the programming language, R, from pre-processing raw tri-axial accelerometery and magnetometry data to VPC dead-reckoning. We have highlighted important considerations to increase the accuracy of the analytical procedure and to avoid misinterpretation of error. We have also supplied extensive supplementary information and supporting functions to aid the process of deriving fine-scale movement paths, including the protocols to correct magnetometry data and derive (tilt-compensated) heading. Importantly, we have demonstrated the value of *Gundog.Tracks*; a multi-functional and user-friendly tool to derive animal movement paths across all media of travel, with detailed input flexibility and output summaries. We suggest the next phase in advancing the utility of animal dead-reckoning includes looking for 'track signatures' that may signify a particular behaviour or reference a particular 'ground-truthed' location. Lastly to advance the utility of

964 *Gundog.Tracks*, we aim to optimise future iterations of the online code to speed up
965 computation time on larger datasets (e.g., sub-second data collected over many months).
966
967
968 ## 5. Declarations
969 Ethics approval and consent to participate
970 We thank the Conservation Agency from the Chubut Province, Argentina for the permits to
971 work at Punta León and Península Valdés protected areas (Disp N° 047/19-SsCyAP). All
972 penguin and cormorant handling procedures were reviewed and approved by the Dirección
973 de Fauna y Flora Silvestre y el Ministerio de Turismo y Áreas Protegidas de la Provincia de
974 Chubut (permits to work at San Lorenzo and Punta León, No. 060/19-DFyFS-MP and No. 047-
975 SsCy/19). Ethical approval was also given by Animal Welfare Ethical Review Body (AWERB),
976 approval number: SU-Ethics-Student-260919/1894, reference: IP-1819-30. Conditions and
977 approvals for lion fieldwork were granted by the Animals Scientific Procedures Act (ASPA) at
978 Queens University of Belfast (QUB-BS-AREC-18-006) and Pretoria University (NAS061-19),
979 permit authorisation was given by South African National Parks (Permit Number SCAM 1550).
980 Consent for publication
981 Not applicable
982 Availability of data and materials
983 We provide a step-by step example R script and an example data file of a Magellanic penguin
984 walking out to sea (with time, raw acceleration and magnetometry data, marked events and
985 aligned GPS positions) to demonstrate some of the key concepts outlined within Section 3
986 when dead-reckoning using *Gundog.Tracks* (including the initial calibration of magnetometry

data with *Gundog.Compass*). All scripts, and the example penguin data file have been uploaded to GitHub [90] and will be made available if the manuscript is accepted for publication. Online scripts will be continually updated and any queries, suggestions and/or reported bugs should be emailed to the corresponding author.

Competing interests

The authors declare no conflict of interest

Funding

This research contributes to the CAASE project funded by King Abdullah University of Science and Technology (KAUST) under the KAUST Sensor Initiative. Fieldwork in the Kgalagadi Transfrontier Park was supported in part by a Department for Economy Global Challenges Research Fund grant to MS. Fieldwork within the Chubut Province was supported in part by the National Agency for Scientific and Technological Promotion of Argentina (PICT 2017 - 1996 and PICT 2018 - 1480), and the Grants-in-Aid for Scientific Research from the Japan Society for the Promotion of Science (16K18617).

Author Contributions

The authors declare no conflict of interest and are in agreement to submit to Animal Biotelemetry. RMG conceived the study and RMG and RW wrote the initial draft. PH constructed tag housings for all model species used. Data collection for the lions was led by SF, DG, PV, LVS and AB and assisted by CJT, MFB, DMS, SB, MVR, PH and RMG. Data collection for the penguins was led by FQ and data collection for the cormorants was led by AGL, with assistance from KY, TY, and RMG. LB, MDH, RPW and RMG conceptualized the key considerations underlying the R code procedures and associated case-studies, and RMG wrote the Gundog scripts and conducted the analysis of the case-studies. MHT supplied data

for the Instantaneous tidal currents of the San Lorenzo region. All authors contributed to manuscript revision and LB, HJW, HME, AGL and LVS contributed to the testing and revision of the R syntax.

Acknowledgments

We thank South African National and the Department of Wildlife and National Parks, Botswana for allowing our research in the Kgalagadi Transfrontier Park. We are grateful to support and kind assistance of the staff and Rangers at the Kgalagadi National Park who were involved with this work, especially Steven Smith, Christa von Elling, Wayne Oppel and Corera Links. Pertaining to the field work carried out in Argentina, we express our gratitude to Andrea Benvenuti, Fabian Gabelli, Monserrat Del Caño, La Chola, Miguel, Estancia El Pedral and Estancia San Lorenzo for assistance in various aspects of the research. We also thank the Instituto de Biología de Organismos Marinos (IBIOMAR-CONICET) for logistical support. HME is funded by an Irish Research Council Government of Ireland postgraduate scholarship.

6. References

1. Cagnacci F, Boitani L, Powell RA, Boyce MS: **Animal ecology meets GPS-based radiotelemetry: a perfect storm of opportunities and challenges**. *Philosophical Transactions of the Royal Society B: Biological Sciences* 2010, **365**(1550):2157-2162.
2. Williams HJ, Taylor LA, Benhamou S, Bijleveld AI, Clay TA, de Grissac S, Demšar U, English HM, Franconi N, Gómez‐Laich A: **Optimizing the use of biologgers for movement ecology research**. *Journal of Animal Ecology* 2020, **89**(1):186-206.
3. Cotter CH: **Early Dead Reckoning Navigation**. *Journal of Navigation* 1978, **31**(1):20-28.
4. Levi RW, Judd T: **Dead reckoning navigational system using accelerometer to measure foot impacts**. In., vol. 5,583,776: Point Research Corporation, Santa Meijer, et al., Methods to Assess Physical Activity with Ana, Calif. ; 1996: 8.
5. Beauregard S, Haas H: **Pedestrian dead reckoning: A basis for personal positioning**. In: *Proceedings of the 3rd Workshop on Positioning, Navigation and Communication: 2006*. 27-35.
6. Walker JS, Jones MW, Laramee RS, Holton MD, Shepard ELC, Williams HJ, Scantlebury DM, Marks NJ, Magowan EA, Maguire IE, Bidder OR, Di Virgilio A, Wilson RP: **Prying into the intimate secrets of animal lives; software beyond hardware for comprehensive annotation in 'Daily Diary' tags**. *Movement Ecology* 2015, **3**(1):29.
7. Bidder OR, Walker JS, Jones MW, Holton MD, Urge P, Scantlebury DM, Marks NJ, Magowan EA, Maguire IE, Wilson RP: **Step by step: reconstruction of terrestrial animal movement paths by dead-reckoning**. *Movement Ecology* 2015, **3**(1):23.
8. Wensveen PJ, Thomas L, Miller PJO: **A path reconstruction method integrating dead-reckoning and position fixes applied to humpback whales**. *Movement Ecology* 2015, **3**(1):31.
9. Andrzejaczek S, Gleiss AC, Lear KO, Pattiaratchi CB, Chapple TK, Meekan MG: **Biologging Tags Reveal Links Between Fine-Scale Horizontal and Vertical Movement Behaviors in Tiger Sharks (Galeocerdo cuvier)**. *Frontiers in Marine Science* 2019, **6**(229).
10. Bowditch N: **The American practical navigator, Bicentennial edition, National Imagery and Mapping Agency, Bethesda, Maryland, 879**. In.; 2002.
11. Wilson R, Wilson M-P: **Dead reckoning: a new technique for determining penguim movements at sea**. *Meeresforschung (Hamburg)* 1988, **32**(2):155-158.
12. Wilson RP, Wilson M-PT, Link R, Mempel H, Adams NJ: **Determination of movements of African penguins *Spheniscus demersus* using a compass system: dead reckoning may be an alternative to telemetry**. *Journal of Experimental Biology* 1991, **157**(1):557-564.
13. Wilson RP, Liebsch N, Davies IM, Quintana F, Weimerskirch H, Storch S, Lucke K, Siebert U, Zankl S, Müller G, Zimmer I, Scolaro A, Campagna C, Plötz J, Bornemann H, Teilmann J, McMahon CR: **All at sea with animal tracks; methodological and analytical solutions for the resolution of movement**. *Deep Sea Research Part II: Topical Studies in Oceanography* 2007, **54**(3):193-210.
14. Mitani Y, Watanabe Y, Sato K, Cameron MF, Naito Y: **3D diving behavior of Weddell seals with respect to prey accessibility and abundance**. *Marine Ecology Progress Series* 2004, **281**:275-281.
15. Elkaim GH, Decker EB, Oliver G, Wright B: **Marine Mammal Marker (MAMMARK) dead reckoning sensor for In-Situ environmental monitoring**. In: *Proceedings of IEEE/ION PLANS 2006: 2006; San Diego, CA*. 976-987.
16. Wilson AD, Wikelski M, Wilson RP, Cooke SJ: **Utility of biological sensor tags in animal conservation**. *Conservation Biology* 2015, **29**(4):1065-1075.

17. Wilson RP, Shepard E, Liebsch N: **Prying into the intimate details of animal lives: use of a daily diary on animals**. *Endangered Species Research* 2008, **4**(1-2):123-137.
18. Pedley M: **eCompass-Build and Calibrate a Tilt-Compensating Electronic Compass**. *Circuit Cellar-The Magazine For Computer Applications* 2012(265):1−6.
19. Li Z, Li X, Wang Y: **A calibration method for magnetic sensors and accelerometer in tilt-compensated digital compass**. In: *2009 9th International Conference on Electronic Measurement & Instruments: 16-19 Aug. 2009 2009*. 2-868-862-871.
20. Ozyagcilar T: **Implementing a tilt-compensated eCompass using accelerometer and magnetometer sensors**. *Freescale semiconductor, Application Note* 2012, **AN4248**.
21. Gheorghe MV, Bodea MC: **Calibration Optimization Study for Tilt-Compensated Compasses**. *IEEE Transactions on Instrumentation and Measurement* 2018, **67**(6):1486-1494.
22. Liu Y, Battaile BC, Trites AW, Zidek JV: **Bias correction and uncertainty characterization of Dead-Reckoned paths of marine mammals**. *Animal Biotelemetry* 2015, **3**(1):51.
23. Dewhirst OP, Evans HK, Roskilly K, Harvey RJ, Hubel TY, Wilson AM: **Improving the accuracy of estimates of animal path and travel distance using GPS drift-corrected dead reckoning**. *Ecology and Evolution* 2016, **6**(17):6210-6222.
24. Mitani Y, Sato K, Ito S, Cameron MF, Siniff DB, Naito Y: **A method for reconstructing three-dimensional dive profiles of marine mammals using geomagnetic intensity data: results from two lactating Weddell seals**. *Polar Biology* 2003, **26**(5):311-317.
25. Whitney NM, Pratt Jr HL, Pratt TC, Carrier JC: **Identifying shark mating behaviour using three-dimensional acceleration loggers**. *Endangered Species Research* 2010, **10**:71-82.
26. Lisovski S, Hewson CM, Klaassen RHG, Korner-Nievergelt F, Kristensen MW, Hahn S: **Geolocation by light: accuracy and precision affected by environmental factors**. *Methods in Ecology and Evolution* 2012, **3**(3):603-612.
27. Miller PJO, Johnson MP, Madsen PT, Biassoni N, Quero M, Tyack PL: **Using at-sea experiments to study the effects of airguns on the foraging behavior of sperm whales in the Gulf of Mexico**. *Deep Sea Research Part I: Oceanographic Research Papers* 2009, **56**(7):1168-1181.
28. Baumgartner MF, Freitag L, Partan J, Ball KR, Prada KE: **Tracking Large Marine Predators in Three Dimensions: The Real-Time Acoustic Tracking System**. *IEEE Journal of Oceanic Engineering* 2008, **33**(2):146-157.
29. Williams LR, Fox DR, Bishop-Hurley GJ, Swain DL: **Use of radio frequency identification (RFID) technology to record grazing beef cattle water point use**. *Computers and Electronics in Agriculture* 2019, **156**:193-202.
30. Alexander JS, Zhang C, Shi K, Riordan P: **A granular view of a snow leopard population using camera traps in Central China**. *Biological Conservation* 2016, **197**:27-31.
31. English HM, Harvey L, Holton MD, Wilson RP, Woodroffe R, Gunner RM, Börger L: **Innovative training and biologgers allow data collection with high conservation value in zoos**. In.; (in prep).
32. Fancy SG, Pank LF, Douglas DC, Curby CH, Garner GW: **Satellite telemetry: a new tool for wildlife research and management**. In. Washington, D.C.: Fish and Wildlife Service Washington DC; 1988.
33. Soutullo A, Cadahía L, Urios V, Ferrer M, Negro JJ: **Accuracy of lightweight satellite telemetry: a case study in the Iberian Peninsula**. *The Journal of Wildlife Management* 2007, **71**(3):1010-1015.
34. Catipovic JA: **Performance limitations in underwater acoustic telemetry**. *IEEE Journal of Oceanic Engineering* 1990, **15**(3):205-216.
35. Hofman MPG, Hayward MW, Heim M, Marchand P, Rolandsen CM, Mattisson J, Urbano F, Heurich M, Mysterud A, Melzheimer J, Morellet N, Voigt U, Allen BL, Gehr B, Rouco C, Ullmann W, Holand Ø, Jørgensen NH, Steinheim G, Cagnacci F, Kroeschel M, Kaczensky P, Buuveibaatar B, Payne JC, Palmegiani I, Jerina K, Kjellander P, Johansson Ö, LaPoint S,

Bayrakcismith R, Linnell JDC, Zaccaroni M, Jorge MLS, Oshima JEF, Songhurst A, Fischer C, Mc Bride RT, Jr., Thompson JJ, Streif S, Sandfort R, Bonenfant C, Drouilly M, Klapproth M, Zinner D, Yarnell R, Stronza A, Wilmott L, Meisingset E, Thaker M, Vanak AT, Nicoloso S, Graeber R, Said S, Boudreau MR, Devlin A, Hoogesteijn R, May-Junior JA, Nifong JC, Odden J, Quigley HB, Tortato F, Parker DM, Caso A, Perrine J, Tellaeche C, Zieba F, Zwijacz-Kozica T, Appel CL, Axsom I, Bean WT, Cristescu B, Périquet S, Teichman KJ, Karpanty S, Licoppe A, Menges V, Black K, Scheppers TL, Schai-Braun SC, Azevedo FC, Lemos FG, Payne A, Swanepoel LH, Weckworth BV, Berger A, Bertassoni A, McCulloch G, Šustr P, Athreya V, Bockmuhl D, Casaer J, Ekori A, Melovski D, Richard-Hansen C, van de Vyver D, Reyna-Hurtado R, Robardet E, Selva N, Sergiel A, Farhadinia MS, Sunde P, Portas R, Ambarli H, Berzins R, Kappeler PM, Mann GK, Pyritz L, Bissett C, Grant T, Steinmetz R, Swedell L, Welch RJ, Armenteras D, Bidder OR, González TM, Rosenblatt A, Kachel S, Balkenhol N: **Right on track? Performance of satellite telemetry in terrestrial wildlife research**. *PLOS ONE* 2019, **14**(5):e0216223.

36. Newey S, Davidson P, Nazir S, Fairhurst G, Verdicchio F, Irvine RJ, van der Wal R: **Limitations of recreational camera traps for wildlife management and conservation research: A practitioner's perspective**. *Ambio* 2015, **44**(4):624-635.

37. Leonardo M, Noss AJ, Erika C, Damián IR: **Ocelot (Felis pardalis) Population Densities, Activity, and Ranging Behaviour in the Dry Forests of Eastern Bolivia: Data from Camera Trapping**. *Journal of Tropical Ecology* 2005, **21**(3):349-353.

38. Lewis JS, Rachlow JL, Garton EO, Vierling LA: **Effects of habitat on GPS collar performance: using data screening to reduce location error**. *Journal of Applied Ecology* 2007, **44**(3):663-671.

39. Kaur M, Sandhu M, Mohan N, Sandhu PS: **RFID technology principles, advantages, limitations & its applications**. *International Journal of Computer and Electrical Engineering* 2011, **3**(1):151.

40. Davis RW, Fuiman LA, Williams TM, Le Boeuf BJ: **Three-dimensional movements and swimming activity of a northern elephant seal**. *Comparative Biochemistry and Physiology Part A: Molecular & Integrative Physiology* 2001, **129**(4):759-770.

41. Wilson RP: **Movements in Adélie Penguins foraging for chicks at Ardley Island, Antarctica: circles within spirals, wheels within wheels**. *Polar Bioscience* 2002(15):75-87.

42. Johnson MP, Tyack PL: **A digital acoustic recording tag for measuring the response of wild marine mammals to sound**. *IEEE Journal of Oceanic Engineering* 2003, **28**(1):3-12.

43. Shiomi K, Sato K, Mitamura H, Arai N, Naito Y, Ponganis PJ: **Effect of ocean current on the dead-reckoning estimation of 3-D dive paths of emperor penguins**. *Aquatic Biology* 2008, **3**(3):265-270.

44. Laplanche C, Marques TA, Thomas L: **Tracking marine mammals in 3D using electronic tag data**. *Methods in Ecology and Evolution* 2015, **6**(9):987-996.

45. Adachi T, Costa DP, Robinson PW, Peterson SH, Yamamichi M, Naito Y, Takahashi A: **Searching for prey in a three-dimensional environment: hierarchical movements enhance foraging success in northern elephant seals**. *Functional Ecology* 2017, **31**(2):361-369.

46. Bras YL, Jouma'a J, Guinet C: **Three-dimensional space use during the bottom phase of southern elephant seal dives**. *Movement Ecology* 2017, **5**(1):18.

47. Andrzejaczek S, Gleiss AC, Pattiaratchi CB, Meekan MG: **First Insights Into the Fine-Scale Movements of the Sandbar Shark, Carcharhinus plumbeus**. *Frontiers in Marine Science* 2018, **5**(483).

48. Aoki K, Amano M, Mori K, Kourogi A, Kubodera T, Miyazaki N: **Active hunting by deep-diving sperm whales: 3D dive profiles and maneuvers during bursts of speed**. *Marine Ecology Progress Series* 2012, **444**:289-301.

49. Narazaki T, Sato K, Abernathy K, Marshall G, Miyazaki N: **Sea turtles compensate deflection of heading at the sea surface during directional travel**. *Journal of Experimental Biology* 2009, **212**(24):4019-4026.

50. Benoit-Bird KJ, Battaile BC, Nordstrom CA, Trites AW: **Foraging behavior of northern fur seals closely matches the hierarchical patch scales of prey**. *Marine Ecology Progress Series* 2013, **479**:283-302.
51. Ware C, Friedlaender AS, Nowacek DP: **Shallow and deep lunge feeding of humpback whales in fjords of the West Antarctic Peninsula**. *Marine Mammal Science* 2011, **27**(3):587-605.
52. Wright BM, Ford JK, Ellis GM, Deecke VB, Shapiro AD, Battaile BC, Trites AW: **Fine-scale foraging movements by fish-eating killer whales (*Orcinus orca*) relate to the vertical distributions and escape responses of salmonid prey (Oncorhynchus spp.)**. *Movement ecology* 2017, **5**(1):1-18.
53. Wensveen PJ, Isojunno S, Hansen RR, von Benda-Beckmann AM, Kleivane L, van IJsselmuide S, Lam F-PA, Kvadsheim PH, DeRuiter SL, Curé C, Narazaki T, Tyack PL, Miller PJO: **Northern bottlenose whales in a pristine environment respond strongly to close and distant navy sonar signals**. *Proceedings of the Royal Society B: Biological Sciences* 2019, **286**(1899):20182592.
54. Goldbogen JA, Calambokidis J, Shadwick RE, Oleson EM, McDonald MA, Hildebrand JA: **Kinematics of foraging dives and lunge-feeding in fin whales**. *Journal of Experimental Biology* 2006, **209**(7):1231-1244.
55. Zimmer WM, Tyack PL, Johnson MP, Madsen PT: **Three-dimensional beam pattern of regular sperm whale clicks confirms bent-horn hypothesis**. *The Journal of the Acoustical Society of America* 2005, **117**(3):1473-1485.
56. Wilson RP, Ropert-Coudert Y, Kato A: **Rush and grab strategies in foraging marine endotherms: the case for haste in penguins**. *Animal Behaviour* 2002, **63**(1):85-95.
57. Gabaldon J, Turner EL, Johnson-Roberson M, Barton K, Johnson M, Anderson EJ, Shorter KA: **Integration, Calibration, and Experimental Verification of a Speed Sensor for Swimming Animals**. *IEEE Sensors Journal* 2019, **19**(10):3616-3625.
58. Denny M: **Air and Water: The Biology and Physics of Life's Media**: Princeton University Press; 1993.
59. Altynay K, Khan Mohammed A, Marengo M, Swanepoel L, Przybysz A, Muller C, Fahlman A, Buttner U, Geraldi NR, Wilson RP, Duarte CM, Kosel J: **Wearable multifunctional printed graphene sensors**. *NPJ Flexible Electronics* 2019, **3**(1).
60. Williams H, Shepard E, Duriez O, Lambertucci SA: **Can accelerometry be used to distinguish between flight types in soaring birds?** *Animal Biotelemetry* 2015, **3**(1):1-11.
61. Williams HJ, Shepard E, Holton MD, Alarcón P, Wilson R, Lambertucci S: **Physical limits of flight performance in the heaviest soaring bird**. *Proceedings of the National Academy of Sciences* 2020, **117**(30):17884-17890.
62. Wilson RP, Börger L, Holton MD, Scantlebury DM, Gómez-Laich A, Quintana F, Rosell F, Graf PM, Williams H, Gunner R, Hopkins L, Marks N, Geraldi NR, Duarte CM, Scott R, Strano MS, Robotka H, Eizaguirre C, Fahlman A, Shepard ELC: **Estimates for energy expenditure in free-living animals using acceleration proxies: A reappraisal**. *Journal of Animal Ecology* 2020, **89**(1):161-172.
63. Bidder OR, Qasem LA, Wilson RP: **On Higher Ground: How Well Can Dynamic Body Acceleration Determine Speed in Variable Terrain?** *PLOS ONE* 2012, **7**(11):e50556.
64. Bidder OR, Soresina M, Shepard ELC, Halsey LG, Quintana F, Gómez-Laich A, Wilson RP: **The need for speed: testing acceleration for estimating animal travel rates in terrestrial dead-reckoning systems**. *Zoology* 2012, **115**(1):58-64.
65. Markovska M, Svensson R: **Evaluation of drift correction strategies for an inertial based dairy cow positioning system. : A study on tracking the position of dairy cows using a foot mounted IMU with drift correction from ZUPT or sparse RFID locations**. *Student thesis.* 2019.

66. di Virgilio A, Morales JM, Lambertucci SA, Shepard EL, Wilson RP: **Multi-dimensional Precision Livestock Farming: a potential toolbox for sustainable rangeland management**. *PeerJ* 2018, **6**:e4867.
67. Shepard EL, Wilson RP, Halsey LG, Quintana F, Laich AG, Gleiss AC, Liebsch N, Myers AE, Norman B: **Derivation of body motion via appropriate smoothing of acceleration data**. *Aquatic Biology* 2008, **4**(3):235-241.
68. Noda T, Okuyama J, Koizumi T, Arai N, Kobayashi M: **Monitoring attitude and dynamic acceleration of free-moving aquatic animals using a gyroscope**. *Aquatic Biology* 2012, **16**(3):265-276.
69. Wilson JW, Mills MG, Wilson RP, Peters G, Mills ME, Speakman JR, Durant SM, Bennett NC, Marks NJ, Scantlebury M: **Cheetahs, *Acinonyx jubatus*, balance turn capacity with pace when chasing prey**. *Biology letters* 2013, **9**(5):20130620.
70. McNarry MA, Wilson RP, Holton MD, Griffiths IW, Mackintosh KA: **Investigating the relationship between energy expenditure, walking speed and angle of turning in humans**. *PLOS ONE* 2017, **12**(8):e0182333.
71. Kaniewski P, Kazubek J: **Integrated system for heading determination**. *Acta Physica Polonica-Series A General Physics* 2009, **116**(3):325.
72. Noda T, Kawabata Y, Arai N, Mitamura H, Watanabe S: **Animal-mounted gyroscope/accelerometer/magnetometer: In situ measurement of the movement performance of fast-start behaviour in fish**. *Journal of Experimental Marine Biology and Ecology* 2014, **451**:55-68.
73. Patonis P, Patias P, Tziavos IN, Rossikopoulos D, Margaritis KG: **A Fusion Method for Combining Low-Cost IMU/Magnetometer Outputs for Use in Applications on Mobile Devices**. *Sensors (Basel, Switzerland)* 2018, **18**(8):2616.
74. Diebel J: **Representing attitude: Euler angles, unit quaternions, and rotation vectors**. In: *Technical Report.* vol. 58. Stanford University, Stanford; 2006: 1-35.
75. Han S, Wang J: **A Novel Method to Integrate IMU and Magnetometers in Attitude and Heading Reference Systems**. *The Journal of Navigation* 2011, **64**(4):727-738.
76. Säll J, Merkel J: **Indoor Navigation Using Accelerometer and Magnetometer**. *Student thesis.* 2011.
77. Alaimo A, Artale V, Milazzo C, Ricciardello A: **Comparison between Euler and quaternion parametrization in UAV dynamics**. *AIP Conference Proceedings* 2013, **1558**(1):1228-1231.
78. Valenti RG, Dryanovski I, Xiao J: **Keeping a good attitude: A quaternion-based orientation filter for IMUs and MARGs**. *Sensors* 2015, **15**(8):19302-19330.
79. Feng K, Li J, Zhang X, Shen C, Bi Y, Zheng T, Liu J: **A New Quaternion-Based Kalman Filter for Real-Time Attitude Estimation Using the Two-Step Geometrically-Intuitive Correction Algorithm**. *Sensors* 2017, **17**(9):2146.
80. Chiella ACB, Teixeira BOS, Pereira GAS: **Quaternion-Based Robust Attitude Estimation Using an Adaptive Unscented Kalman Filter**. *Sensors* 2019, **19**(10):2372.
81. Gunner RM, Wilson RP, Holton MD, Scott R, Hopkins P, Duarte CM: **A new direction for differentiating animal activity based on measuring angular velocity about the yaw axis**. *Ecology and Evolution* 2020, **10**(14):7872-7886.
82. Wiltschko R: **Magnetic orientation in animals**, vol. 33. Berlin Heidelberg: Springer Science & Business Media; 2012.
83. Sequeira MM, Rickenbach M, Wietlisbach V, Tullen B, Schutz Y: **Physical Activity Assessment Using a Pedometer and Its Comparison with a Questionnaire in a Large Population Survey**. *American Journal of Epidemiology* 1995, **142**(9):989-999.
84. Kerdok AE, Biewener AA, McMahon TA, Weyand PG, Herr HM: **Energetics and mechanics of human running on surfaces of different stiffnesses**. *Journal of Applied Physiology* 2002, **92**(2):469-478.

85. Halsey LG, Shepard ELC, Hulston CJ, Venables MC, White CR, Jeukendrup AE, Wilson RP: **Acceleration versus heart rate for estimating energy expenditure and speed during locomotion in animals: Tests with an easy model species, Homo sapiens**. *Zoology* 2008, **111**(3):231-241.
86. Miwa M, Oishi K, Nakagawa Y, Maeno H, Anzai H, Kumagai H, Okano K, Tobioka H, Hirooka H: **Application of Overall Dynamic Body Acceleration as a Proxy for Estimating the Energy Expenditure of Grazing Farm Animals: Relationship with Heart Rate**. *PLOS ONE* 2015, **10**(6):e0128042.
87. Chapman Jason W, Klaassen Raymond HG, Drake VA, Fossette S, Hays Graeme C, Metcalfe Julian D, Reynolds Andrew M, Reynolds Don R, Alerstam T: **Animal Orientation Strategies for Movement in Flows**. *Current Biology* 2011, **21**(20):R861-R870.
88. R Development Core Team: **R - A language and environment for statistical computing**. In. Vienna, Austria: R Foundation for Statistical Computing; 2021.
89. **The R Project for Statistical Computing. Available at https://www.r-project.org/. Accessed 07 March 2021**.
90. **Gundog.Tracks GitHub database. Available at https://github.com/Richard6195/Gundog.Dead-Reckoning.git. Accessed 07 March 2021**
91. Gunner RM, Wilson RP, Holton MD, Hopkins P, Bell SH, Marks NJ, Bennett NC, Ferreira S, Govender D, Viljoen P, Bruns A, Schalkwyk Lv, Bertelsen MF, Duarte CM, Rooyen MCv, Tambling CJ, Goppert A, Diesel D, Scantlebury DM: **Decision rules for determining terrestrial movement and the consequences for filtering high-resolution GPS tracks – A case study using the African Lion (*Panthera leo*)**. (in review).
92. Dunford CE, Marks NJ, Wilmers CC, Bryce CM, Nickel B, Wolfe LL, Scantlebury DM, Williams TM: **Surviving in steep terrain: a lab-to-field assessment of locomotor costs for wild mountain lions (Puma concolor)**. *Movement Ecology* 2020, **8**(1):34.
93. Wilson RP, Rose KA, Gunner R, Holton M, Marks NJ, Bennett NC, Bell SH, Twining JP, Hesketh J, Duarte CM, Bezodis N, Scantlebury DM: **Forces experienced by instrumented animals depend on lifestyle**. *bioRxiv* 2020:2020.2008.2020.258756.
94. Willener AST, Handrich Y, Halsey LG, Strike S: **Effect of walking speed on the gait of king penguins: An accelerometric approach**. *Journal of Theoretical Biology* 2015, **387**:166-173.
95. Wilson RP, Holton MD, di Virgilio A, Williams H, Shepard ELC, Lambertucci S, Quintana F, Sala JE, Balaji B, Lee ES, Srivastava M, Scantlebury DM, Duarte CM: **Give the machine a hand: A Boolean time-based decision-tree template for rapidly finding animal behaviours in multisensor data**. *Methods in Ecology and Evolution* 2018, **9**(11):2206-2215.
96. Rong L, Zhiguo D, Jianzhong Z, Ming L: **Identification of Individual Walking Patterns Using Gait Acceleration**. In: *2007 1st International Conference on Bioinformatics and Biomedical Engineering: 6-8 July 2007 2007*. 543-546.
97. Wilson RP, Hustler K, Ryan PG, Burger AE, Noldeke EC: **Diving birds in cold water: do Archimedes and Boyle determine energetic costs?** *The American Naturalist* 1992, **140**(2):179-200.
98. Williams HJ, Holton MD, Shepard ELC, Largey N, Norman B, Ryan PG, Duriez O, Scantlebury M, Quintana F, Magowan EA, Marks NJ, Alagaili AN, Bennett NC, Wilson RP: **Identification of animal movement patterns using tri-axial magnetometry**. *Movement Ecology* 2017, **5**(1):6.
99. Whitford M, Klimley AP: **An overview of behavioral, physiological, and environmental sensors used in animal biotelemetry and biologging studies**. *Animal Biotelemetry* 2019, **7**(1):1-24.
100. Shamoun-Baranes J, Bom R, van Loon EE, Ens BJ, Oosterbeek K, Bouten W: **From Sensor Data to Animal Behaviour: An Oystercatcher Example**. *PLOS ONE* 2012, **7**(5):e37997.
101. Wilson R: **The Jackass Penguin (Spheniscus demersus) as a pelagic predator**. *Marine Ecology Progress Series* 1985, **25**(3):219-227.

102. Culik BM, Wilson RP, Dannfeld R, Adelung D, Spairani HJ, Coria NRC: **Pygoscelid penguins in a swim canal**. *Polar Biology* 1991, **11**(4):277-282.
103. Bethge P, Nicol S, Culik BM, Wilson RP: **Diving behaviour and energetics in breeding little penguins (Eudyptula minor)**. *Journal of Zoology* 1997, **242**(3):483-502.
104. Tobalske B, Dial K: **Flight kinematics of black-billed magpies and pigeons over a wide range of speeds**. *Journal of Experimental Biology* 1996, **199**(2):263-280.
105. Sato K, Sakamoto KQ, Watanuki Y, Takahashi A, Katsumata N, Bost C-A, Weimerskirch H: **Scaling of Soaring Seabirds and Implications for Flight Abilities of Giant Pterosaurs**. *PLOS ONE* 2009, **4**(4):e5400.
106. Scharold J, Lai NC, Lowell W, Graham J: **Metabolic rate, heart rate, and tailbeat frequency during sustained swimming in the leopard shark Triakis semifasciata**. *Experimental biology* 1989, **48**(4):223-230.
107. Kawabe R, Kawano T, Nakano N, Yamashita N, Hiraishi T, Naito Y: **Simultaneous measurement of swimming speed and tail beat activity of free-swimming rainbow trout *Oncorhynchus mykiss* using an acceleration data-logger**. *Fisheries science* 2003, **69**(5):959-965.
108. Steinhausen MF, Steffensen JF, Andersen NG: **Tail beat frequency as a predictor of swimming speed and oxygen consumption of saithe (Pollachius virens) and whiting (*Merlangius merlangus*) during forced swimming**. *Marine Biology* 2005, **148**(1):197-204.
109. Miller PJO, Johnson MP, Tyack PL, Terray EA: **Swimming gaits, passive drag and buoyancy of diving sperm whales Physeter macrocephalus**. *Journal of Experimental Biology* 2004, **207**(11):1953-1967.
110. Laich AG, Wilson RP, Quintana F, Shepard EL: **Identification of imperial cormorant Phalacrocorax atriceps behaviour using accelerometers**. *Endangered species research* 2008, **10**:29-37.
111. Chakravarty P, Cozzi G, Ozgul A, Aminian K: **A novel biomechanical approach for animal behaviour recognition using accelerometers**. *Methods in Ecology and Evolution* 2019, **10**(6):802-814.
112. Chakravarty P, Maalberg M, Cozzi G, Ozgul A, Aminian K: **Behavioural compass: animal behaviour recognition using magnetometers**. *Movement Ecology* 2019, **7**(1):28.
113. Hochscheid S: **Why we mind sea turtles' underwater business: A review on the study of diving behavior**. *Journal of Experimental Marine Biology and Ecology* 2014, **450**:118-136.
114. Constandache I, Bao X, Azizyan M, Choudhury RR: **Did you see Bob? human localization using mobile phones**. In: *Proceedings of the sixteenth annual international conference on Mobile computing and networking; Chicago, Illinois, USA*. Association for Computing Machinery 2010: 149–160.
115. Symington A, Trigoni N: **Encounter based sensor tracking**. In: *Proceedings of the thirteenth ACM international symposium on Mobile Ad Hoc Networking and Computing; Hilton Head, South Carolina, USA*. Association for Computing Machinery 2012: 15–24.
116. Harja YD, Sarno R: **Determine the best option for nearest medical services using Google maps API, Haversine and TOPSIS algorithm**. In: *2018 International Conference on Information and Communications Technology (ICOIACT): 6-7 March 2018 2018*. 814-819.
117. **Great circle distances and bearings between two locations** [https://dtcenter.org/met/users/docs/write_ups/gc_simple.pdf]
118. Robusto CC: **The Cosine-Haversine Formula**. *The American Mathematical Monthly* 1957, **64**(1):38-40.
119. Zeileis A, Grothendieck G, Ryan JA, Andrews F, Zeileis MA: **Package 'zoo'**. 2020.
120. Jockers ML, Thalken R: **Introduction to dplyr**. In: *Text Analysis with R for Students of Literature.* Switzerland: Springer, Cham; 2020: 121-132.

121. **Calculating Azimuth, Distance, and Altitude from a Pair of GPS Locations in JavaScript** [https://medium.com/javascript-in-plain-english/calculating-azimuth-distance-and-altitude-from-a-pair-of-gps-locations-36b4325d8ab0]
122. Handcock RN, Swain DL, Bishop-Hurley GJ, Patison KP, Wark T, Valencia P, Corke P, O'Neill CJ: **Monitoring Animal Behaviour and Environmental Interactions Using Wireless Sensor Networks, GPS Collars and Satellite Remote Sensing**. *Sensors* 2009, **9**(5):3586-3603.
123. Gužvica G, Bošnjak I, Bielen A, Babić D, Radanović-Gužvica B, Šver L: **Comparative Analysis of Three Different Methods for Monitoring the Use of Green Bridges by Wildlife**. *PLOS ONE* 2014, **9**(8):e106194.
124. Patel A, Stocks B, Fisher C, Nicolls F, Boje E: **Tracking the Cheetah Tail Using Animal-Borne Cameras, GPS, and an IMU**. *IEEE Sensors Letters* 2017, **1**(4):1-4.
125. Latham ADM, Latham MC, Anderson DP, Cruz J, Herries D, Hebblewhite M: **The GPS craze: six questions to address before deciding to deploy GPS technology on wildlife**. *New Zealand Journal of Ecology* 2015, **39**(1):143-152.
126. Hebblewhite M, Haydon DT: **Distinguishing technology from biology: a critical review of the use of GPS telemetry data in ecology**. *Philosophical Transactions of the Royal Society B: Biological Sciences* 2010, **365**(1550):2303-2312.
127. Gibb R, Shoji A, Fayet AL, Perrins CM, Guilford T, Freeman R: **Remotely sensed wind speed predicts soaring behaviour in a wide-ranging pelagic seabird**. *Journal of The Royal Society Interface* 2017, **14**(132):20170262.
128. Swain DL, Wark T, Bishop-Hurley GJ: **Using high fix rate GPS data to determine the relationships between fix rate, prediction errors and patch selection**. *Ecological Modelling* 2008, **212**(3):273-279.
129. Ryan PG, Petersen SL, Peters G, Grémillet D: **GPS tracking a marine predator: the effects of precision, resolution and sampling rate on foraging tracks of African Penguins**. *Marine Biology* 2004, **145**(2):215-223.
130. Bouvet D, Garcia G: **GPS latency identification by Kalman filtering**. *Robotica* 2000, **18**(5):475-485.
131. Frair JL, Fieberg J, Hebblewhite M, Cagnacci F, DeCesare NJ, Pedrotti L: **Resolving issues of imprecise and habitat-biased locations in ecological analyses using GPS telemetry data**. *Philosophical Transactions of the Royal Society B: Biological Sciences* 2010, **365**(1550):2187-2200.
132. Péron G, Calabrese JM, Duriez O, Fleming CH, García-Jiménez R, Johnston A, Lambertucci SA, Safi K, Shepard ELC: **The challenges of estimating the distribution of flight heights from telemetry or altimetry data**. *Animal Biotelemetry* 2020, **8**(1):5.
133. Poulin M-P, Clermont J, Berteaux D: **Extensive daily movement rates measured in territorial arctic foxes**. *Ecology and Evolution* 2021, **00**:1– 12.
134. Marcus Rowcliffe J, Carbone C, Kays R, Kranstauber B, Jansen PA: **Bias in estimating animal travel distance: the effect of sampling frequency**. *Methods in Ecology and Evolution* 2012, **3**(4):653-662.
135. Belant JL: **Effects of Antenna Orientation and Vegetation on Global Positioning System Telemetry Collar Performance**. *Northeastern Naturalist* 2009, **16**(4):577-584, 578.
136. Graf PM, Wilson RP, Qasem L, Hackländer K, Rosell F: **The Use of Acceleration to Code for Animal Behaviours; A Case Study in Free-Ranging Eurasian Beavers Castor fiber**. *PLOS ONE* 2015, **10**(8):e0136751.
137. Tonini MH, Palma ED: **Tidal dynamics on the North Patagonian Argentinean Gulfs**. *Estuarine, Coastal and Shelf Science* 2017, **189**:115-130.
138. Wilson RP, Kreye JM, Lucke K, Urquhart H: **Antennae on transmitters on penguins: balancing energy budgets on the high wire**. *Journal of Experimental biology* 2004, **207**(15):2649-2662.

139. McClune DW: **Joining the dots: reconstructing 3D environments and movement paths using animal-borne devices**. *Animal Biotelemetry* 2018, **6**(1):5.
140. Wilson R, Griffiths I, Legg P, Friswell M, Bidder O, Halsey L, Lambertucci SA, Shepard E: **Turn costs change the value of animal search paths**. *Ecology Letters* 2013, **16**(9):1145-1150.
141. Potts J, Börger L, Scantlebury DM, Bennett NC, Alagaili A, Wilson RP: **Finding turning-points in ultra-high-resolution animal movement data**. *Methods in Ecology and Evolution* 2018, **9**(10):2091-2101.
142. Dowle M, Srinivasan A, Gorecki J, Chirico M, Stetsenko P, Short T, Lianoglou S, Antonyan E, Bonsch M, Parsonage H: **Package 'data. table'**. *Extension of 'data frame* 2019.
143. Kunčar A, Sysel M, Urbánek T: **Calibration of low-cost triaxial magnetometer**. In: *MATEC Web of Conferences 20th International Conference on Circuits, Systems, Communications and Computers (CSCC 2016): 2016*. EDP Sciences.
144. Sodhi R, Prunty J, Hsu G, Oh B: **Automatic calibration of a three-axis magnetic compass**. In., vol. U.S. Patent 7,451,549 PNI Corporation (Santa Rosa, CA, US); 2008.
145. Renaudin V, Afzal MH, Lachapelle G: **Complete Triaxis Magnetometer Calibration in the Magnetic Domain**. *Journal of Sensors* 2010, **2010**:967245.
146. Tabatabaei SAH, Gluhak A, Tafazolli R: **A Fast Calibration Method for Triaxial Magnetometers**. *IEEE Transactions on Instrumentation and Measurement* 2013, **62**(11):2929-2937.
147. Vitali A: **Ellipsoid or sphere fitting for sensor calibration, Dt0059**. *ST Microelectronics, Design Tip* 2016.
148. **Simple and Effective Magnetometer Calibration** [https://github.com/kriswiner/MPU6050/wiki/Simple-and-Effective-Magnetometer-Calibration]
149. Gleiss AC, Wilson RP, Shepard ELC: **Making overall dynamic body acceleration work: on the theory of acceleration as a proxy for energy expenditure**. *Methods in Ecology and Evolution* 2011, **2**(1):23-33.
150. Choi S, Youn I-H, LeMay R, Burns S, Youn J-H: **Biometric gait recognition based on wireless acceleration sensor using k-nearest neighbor classification**. In: *2014 International Conference on Computing, Networking and Communications (ICNC): 3-6 Feb. 2014 2014*. 1091-1095.
151. Sato K, Mitani Y, Cameron MF, Siniff DB, Naito Y: **Factors affecting stroking patterns and body angle in diving Weddell seals under natural conditions**. *Journal of Experimental Biology* 2003, **206**(9):1461-1470.
152. Li W, Wang J: **Effective Adaptive Kalman Filter for MEMS-IMU/Magnetometers Integrated Attitude and Heading Reference Systems**. *Journal of Navigation* 2013, **66**(1):99-113.
153. Pedley M: **Tilt sensing using a three-axis accelerometer**. *Freescale semiconductor Application Note 2461* 2013, **1**(Rev. 6):1–22.
154. Caruso MJ: **Applications of magnetic sensors for low cost compass systems**. In: *IEEE 2000 Position Location and Navigation Symposium (Cat No00CH37062): 13-16 March 2000 2000*. 177-184.
155. Boelter KDH: **Aircraft Magnetic Declinator System**. In., vol. 2020/0182619: The Boeing Company , Chicago , IL (US) 2020.
156. **World Magnetic Model 2020 Calculator. Available at http://www.geomag.bgs.ac.uk/data_service/models_compass/wmm_calc.html. Accessed 07 March 2021**.
157. Qasem L, Cardew A, Wilson A, Griffiths I, Halsey LG, Shepard ELC, Gleiss AC, Wilson R: **Tri-Axial Dynamic Acceleration as a Proxy for Animal Energy Expenditure; Should We Be Summing Values or Calculating the Vector?** *PLOS ONE* 2012, **7**(2):e31187.
158. Pewsey A, Neuhäuser M, Ruxton GD: **Circular Statistics in R**: OUP Oxford; 2013.

159. Farrahi V, Niemelä M, Kangas M, Korpelainen R, Jämsä T: **Calibration and validation of accelerometer-based activity monitors: A systematic review of machine-learning approaches**. *Gait & Posture* 2019, **68**:285-299.
160. Ropert-Coudert Y, Kato A, Baudat J, Bost C-A, Le Maho Y, Naito Y: **Time/depth usage of Adélie penguins: an approach based on dive angles**. *Polar Biology* 2001, **24**(6):467-470.
161. **Movable Type Scripts. Available at https://www.movable-type.co.uk/scripts/latlong.html. Accessed 07 March 2021**.
162. Grolemund G, Wickham H: **Dates and times made easy with lubridate**. *Journal of statistical software* 2011, **40**(i03):1-25.

1512 # Figure legends

Figure 1. Schematic representation of a current flow vector (orange) (due to its speed and direction) being integrated to a given travel vector (blue). The x,y reflect the initial location of a dead-reckoned track, x2 and y2 are the resultant location following the integration of a travel vector (prior to current integration) and xxx and yyy advance these x2 and y2 values a step further in the direction of the wind vector. The dashed lines indicate the magnitude of the x and y dimensions of travel (both pre- and post-current flow integration) and the green line reflects the actual travel vector.

Figure 2. Schematic of the conceptual workflow involved when dead-reckoning using Gundog.Tracks – elaborated within section 3. Note Gundog.Peaks is a peak finder function that locates peaks based on local signal maxima and Gundog.Compass is a function to correct iron distortions from tri-axial magnetometry data and subsequently compute tilt-compensated heading. Both functions are elaborated within section 3 and SI. The direction of workflow and key questions ask follows from green- (pre-processing and data alignment) to purple- (computing heading) sections, before splitting into blue- (air/water) and brown- (land) sections (computing speed) and culminating at the red section (final pre-dead reckoning checks/data formats & post-dead-reckoning checks/plots) in conjunction with the process of using Gundog.Tracks in R (yellow).

Figure 3. Dead-reckoned (DR) movement path of lion as provided by Gundog.Tracks summary plots (within the initialised R graphics window). This is an approximate two-week trajectory over an approximated total travel (DR) distance of > 142 km. (Pre-filtered) GPS (red) was sampled at 1 Hz and derived heading and speed measurements were sub-sampled to 1Hz (initial acceleration/magnetometry data were recorded at 40 Hz). The VPC dead-reckoned track (blue) was constructed using DBA~GPS-derived speed regression estimates and corrected approx. every 6 hours. Note, for dead-reckoning within fluid media, an additional green dead-reckoned track with current integration and its associated distance estimates are also plotted (pre-correction) when wind/ocean currents are supplied (cf. Fig. 6). Accumulated 3-D DR distance is shown when elevation/depth data is supplied.

*Figure 4. Net error between (GPS-corrected) dead-reckoned and GPS positions for a track from 5 African lions. (a) Maximum net error (m) between ground-truthed GPS and time-matched dead-reckoned positions after one iteration of correction, both as a function of GPS correction rate (one correction per 1 (red), 12 (green) and 24 (blue) hours) and underlying m coefficient used to determine the DBA-derived speed. Data from 5 lions (individual denoted by symbol shape) over a period of 12 days. Note that the difference in error varies according to individual, initial speed estimate and the scale of correction. (b) Net error between dead-reckoned positions and all available GPS fixes (data from the same 5 lions), subsequent to the iterative procedure of GPS correction (maximum distance between GPS fix used in correction procedure and according dead-reckoned position < .01 m). Boxes denote the median and 25-75 % interquartile range with a blue 'loess' smooth line. Whiskers extend to 1.5 * Interquartile range in both directions.*

Figure 5. Dead reckoned lion track in relation to GPS positions ((a) = uncorrected & (b) = corrected – approx. every 30 mins (black circles)). The start of the track (lo and la) is denoted with a black x. Three corresponding sections of each track are denoted with the same number and the finishing positions denoted with a circle (coloured according to the reference track). Note that the horizontal straight-line sections (cf. yellow arrow) result from the lion following the Botswana boundary fence (which this individual eventually crossed). Mean net error between (corrected) dead-reckoned positions and all available GPS fixes was higher for tracks resolved using a VeDBA threshold (0.11 g), relative to depicted movement.

Figure 6. One Magellanic penguin's dead-reckoned foraging trip at sea, lasting approximately 9 hours (yellow arrow denotes the trajectory direction over time. Black track = GPS. Fifteen corrections (black circles) were made (method = "divide"). For comparison, the grey dotted track is the GPS corrected dead-reckoned track with current integration approx. every 1 min (where possible - method = "time") (a). Note the difference of net error between dead-reckoned positions and all available GPS fixes across the various tracks [insert = grey track] (b). Both uncorrected and corrected dead-reckoned tracks had less error subsequent to current integration (black arrows vector every 5 mins) and this was reflected in the direction and magnitude of heading correction factors required per unit time (c). Heading correction factors obtained from the track corrected approx. every 1 min; the colour of the scale bar indicates the extent of the heading correction factor required).

Figure 7. Twelve outgoing (green) and incoming (blue) dead-reckoned trajectories from Magellanic penguins walking to and from their nest. Three variants of track advancement were used; (a) A VeDBA threshold (0.1 g) and constant m-coefficient (1.4) (b), depicted movement periods using the LoCoD method to identify steps (cf. Wilson et al. 2018) and constant m-coefficient (1.4) and (c) depicted individual steps within depicted movement periods, from which a constant distance estimate (0.16 m) was multiplied by step frequency ($\bar{x}$ no. steps/s) (full details within SI_4) (c). Note that the accuracy with respect to the radial distance can be evaluated by examining the track stops in relation to the shore-line. Tracks (from (c)) were GPS-corrected (d) (method = "distance", dist.step = 5, VP.ME = TRUE, thresh = between 8-15 (depending on track length)) approx. every 50 m). A portion of the GPS-corrected dead-reckoned tracks (bottom panel) are magnified (2 iterations) to show the difference in resolution of movement tortuosity, between GPS and dead-reckoned tracks.

Figure 8. GPS-corrected dead-reckoned tracks of Imperial cormorants foraging at sea; (a) 15 birds (blue = male, red = female). (b) shows one of these tracks illustrated in 3-D. Note gaps between dives are either associated with current drift, while the bird is resting at the sea surface, or periods of flight. (c) and (d) show the descent, bottom phase and ascent of a given dive in both 2-D (c) and 3-D, respectively.

Figure 9. Schematic diagram illustrating the order of fixes used when calculating the $Distance_{corr.factor}$ *and* $Heading_{corr.factor}$ *(difference of both GPS and dead-reckoned (DR) positions between arrow heads). Note the discrepancy with the order at which these correction factors are applied to intermediate DR positions (as denoted by colour shading). Known starting position denoted with *.*

Figures

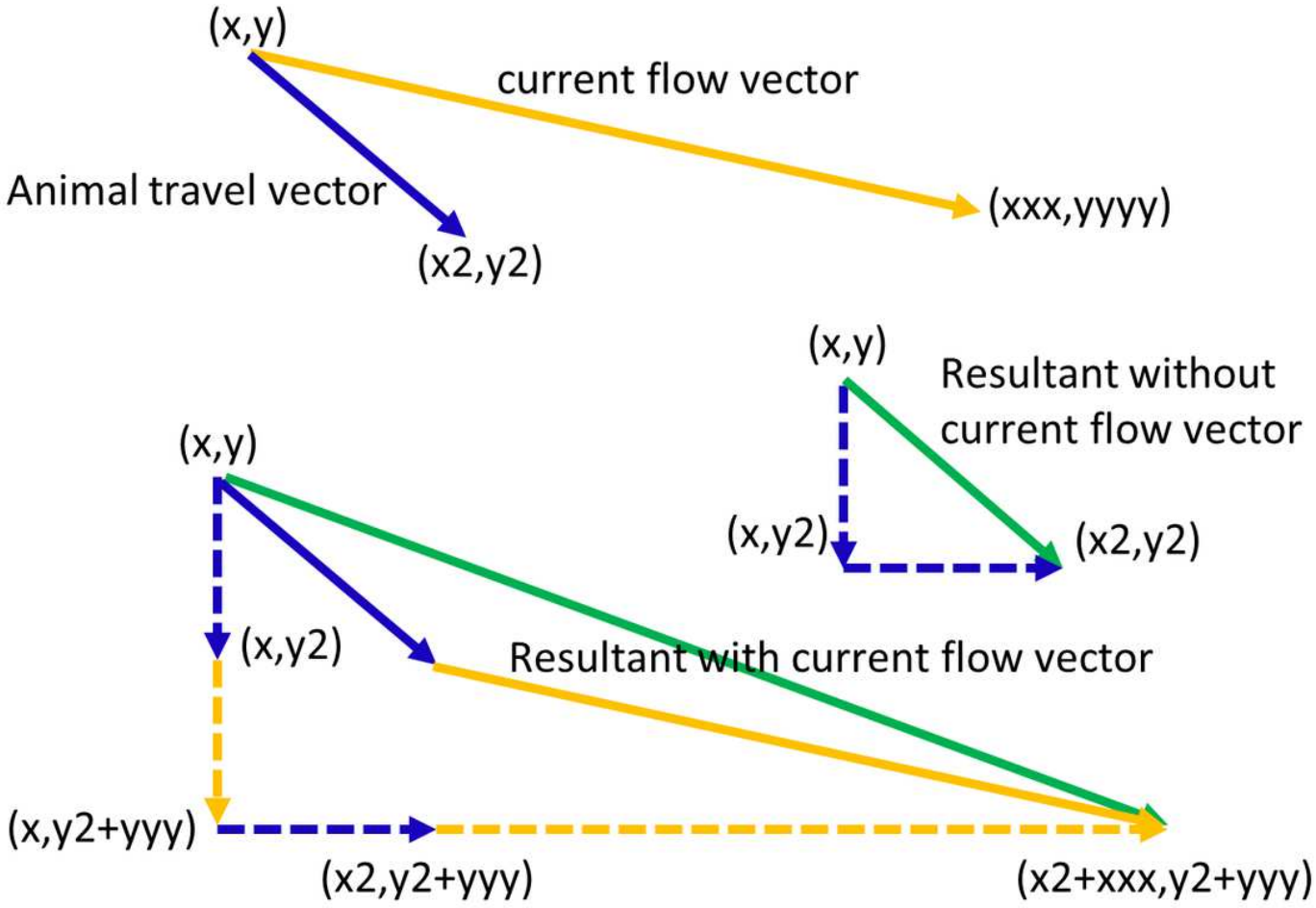

Figure 1

Schematic representation of a current flow vector (orange) (due to its speed and direction) being integrated to a given travel vector (blue). The x,y reflect the initial location of a dead-reckoned track, x2 and y2 are the resultant location following the integration of a travel vector (prior to current integration) and xxx and yyy advance these x2 and y2 values a step further in the direction of the wind vector. The dashed lines indicate the magnitude of the x and y dimensions of travel (both pre- and post-current flow integration) and the green line reflects the actual travel vector.

Figure 2

Schematic of the conceptual workflow involved when dead-reckoning using Gundog.Tracks – elaborated within section 3. Note Gundog.Peaks is a peak finder function that locates peaks based on local signal maxima and Gundog.Compass is a function to correct iron distortions from tri-axial magnetometry data and subsequently compute tilt-compensated heading. Both functions are elaborated within section 3 and SI. The direction of workflow and key questions ask follows from green- (pre-processing and data alignment) to purple- (computing heading) sections, before splitting into blue- (air/water) and brown- (land) sections (computing speed) and culminating at the red section (final pre-dead reckoning

checks/data formats & post-dead-reckoning checks/plots) in conjunction with the process of using Gundog.Tracks in R (yellow).

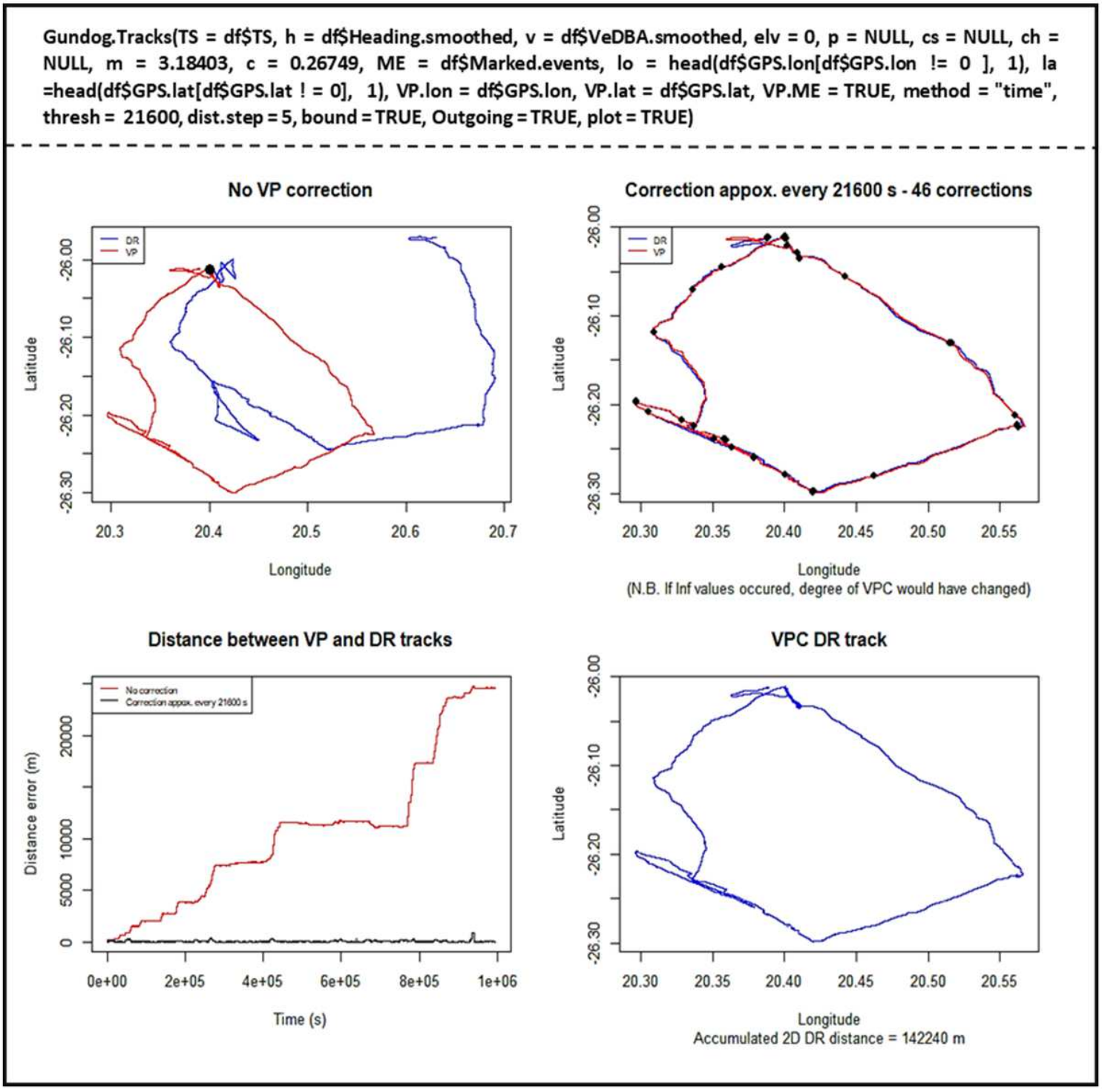

Figure 3

Dead-reckoned (DR) movement path of lion as provided by Gundog.Tracks summary plots (within the initialised R graphics window). This is an approximate two-week trajectory over an approximated total travel (DR) distance of > 142 km. (Pre-filtered) GPS (red) was sampled at 1 Hz and derived heading and speed measurements were sub-sampled to 1Hz (initial acceleration/magnetometry data were recorded at

40 Hz). The VPC dead-reckoned track (blue) was constructed using DBA~GPS-derived speed regression estimates and corrected approx. every 6 hours. Note, for dead-reckoning within fluid media, an additional green dead-reckoned track with current integration and its associated distance estimates are also plotted (pre-correction) when wind/ocean currents are supplied (cf. Fig. 6). Accumulated 3-D DR distance is shown when elevation/depth data is supplied. Note: The designations employed and the presentation of the material on this map do not imply the expression of any opinion whatsoever on the part of Research Square concerning the legal status of any country, territory, city or area or of its authorities, or concerning the delimitation of its frontiers or boundaries. This map has been provided by the authors.

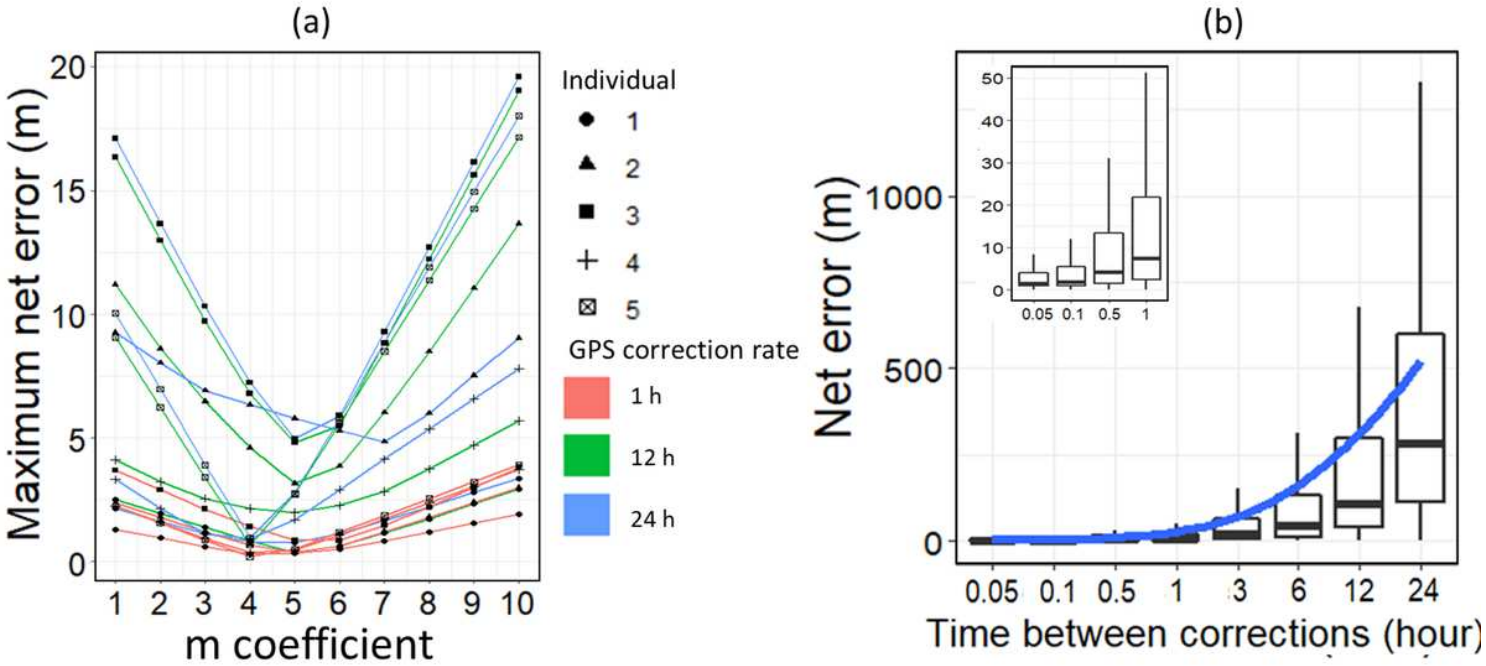

Figure 4

Net error between (GPS-corrected) dead-reckoned and GPS positions for a track from 5 African lions. (a) Maximum net error (m) between ground-truthed GPS and time-matched dead-reckoned positions after one iteration of correction, both as a function of GPS correction rate (one correction per 1 (red), 12 (green) and 24 (blue) hours) and underlying m coefficient used to determine the DBA-derived speed. Data from 5 lions (individual denoted by symbol shape) over a period of 12 days. Note that the difference in error varies according to individual, initial speed estimate and the scale of correction. (b) Net error between dead-reckoned positions and all available GPS fixes (data from the same 5 lions), subsequent to the iterative procedure of GPS correction (maximum distance between GPS fix used in correction procedure and according dead-reckoned position < .01 m). Boxes denote the median and 25-75 % interquartile range with a blue 'loess' smooth line. Whiskers extend to 1.5 * Interquartile range in both directions.

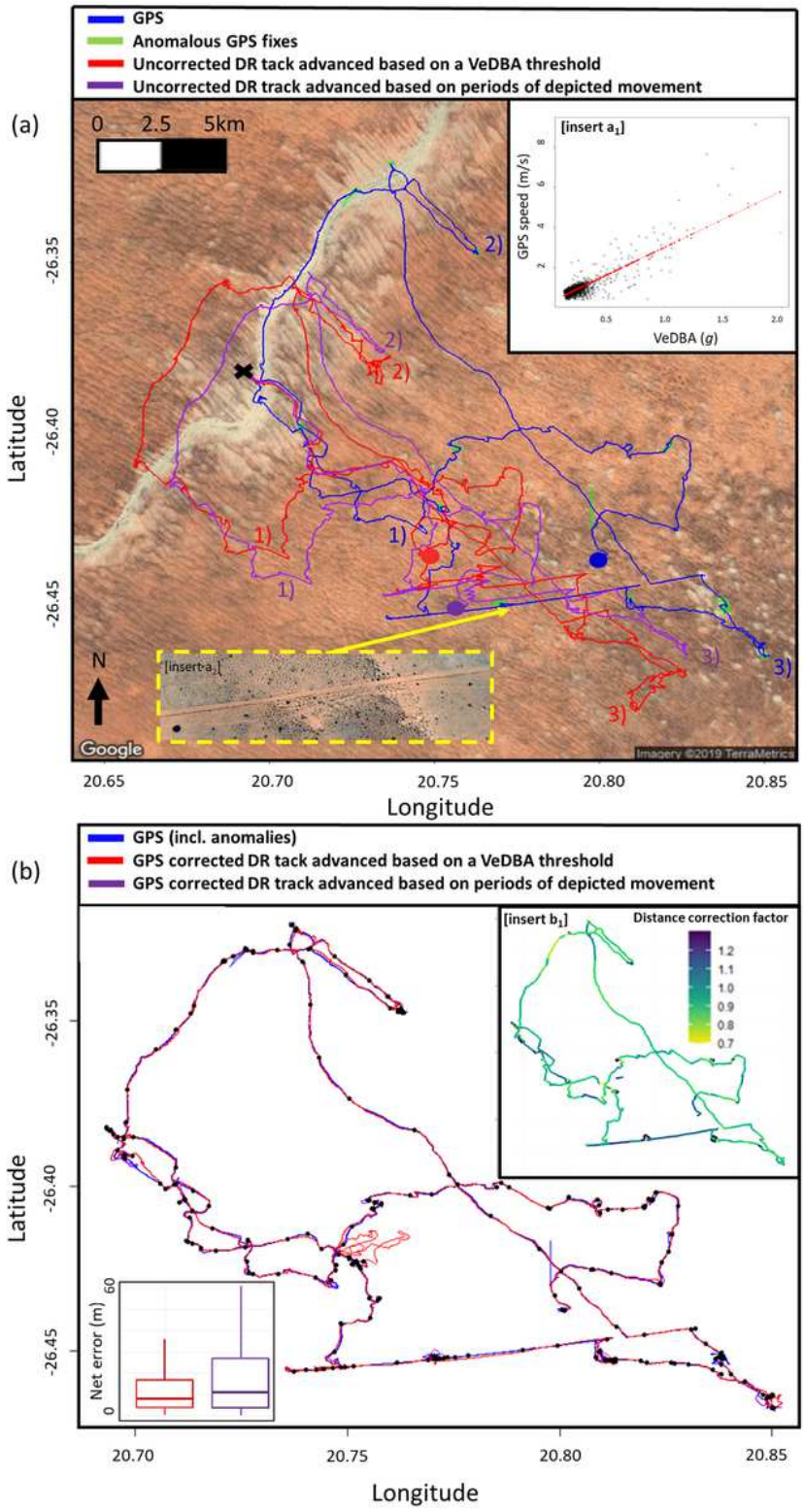

Figure 5

Dead reckoned lion track in relation to GPS positions ((a) = uncorrected & (b) = corrected – approx. every 30 mins (black circles)). The start of the track (lo and la) is denoted with a black x. Three corresponding sections of each track are denoted with the same number and the finishing positions denoted with a circle (coloured according to the reference track). Note that the horizontal straight-line sections (cf. yellow arrow) result from the lion following the Botswana boundary fence (which this individual eventually

crossed). Mean net error between (corrected) dead-reckoned positions and all available GPS fixes was higher for tracks resolved using a VeDBA threshold (0.11 g), relative to depicted movement. Note: The designations employed and the presentation of the material on this map do not imply the expression of any opinion whatsoever on the part of Research Square concerning the legal status of any country, territory, city or area or of its authorities, or concerning the delimitation of its frontiers or boundaries. This map has been provided by the authors.

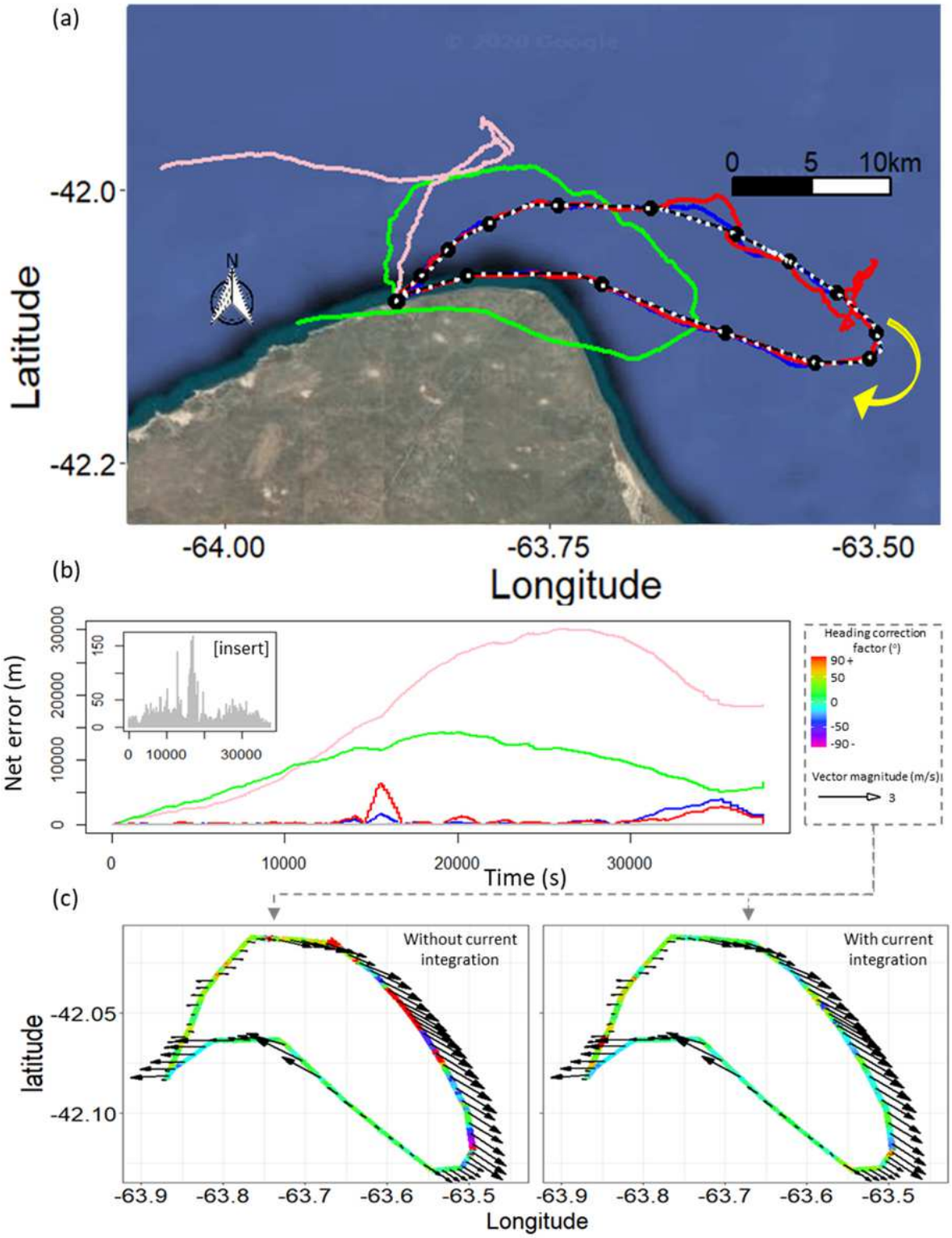

Figure 6

One Magellanic penguin’s dead-reckoned foraging trip at sea, lasting approximately 9 hours (yellow arrow denotes the trajectory direction over time. Black track = GPS. Fifteen corrections (black circles) were made (method = “divide”). For comparison, the grey dotted track is the GPS corrected dead-reckoned track with current integration approx. every 1 min (where possible - method = “time”) (a). Note the difference of net error between dead-reckoned positions and all available GPS fixes across the various tracks [insert = grey track] (b). Both uncorrected and corrected dead-reckoned tracks had less error subsequent to current integration (black arrows vector every 5 mins) and this was reflected in the direction and magnitude of heading correction factors required per unit time (c). Heading correction factors obtained from the track corrected approx. every 1 min; the colour of the scale bar indicates the extent of the heading correction factor required). Note: The designations employed and the presentation of the material on this map do not imply the expression of any opinion whatsoever on the part of Research Square concerning the legal status of any country, territory, city or area or of its authorities, or concerning the delimitation of its frontiers or boundaries. This map has been provided by the authors.

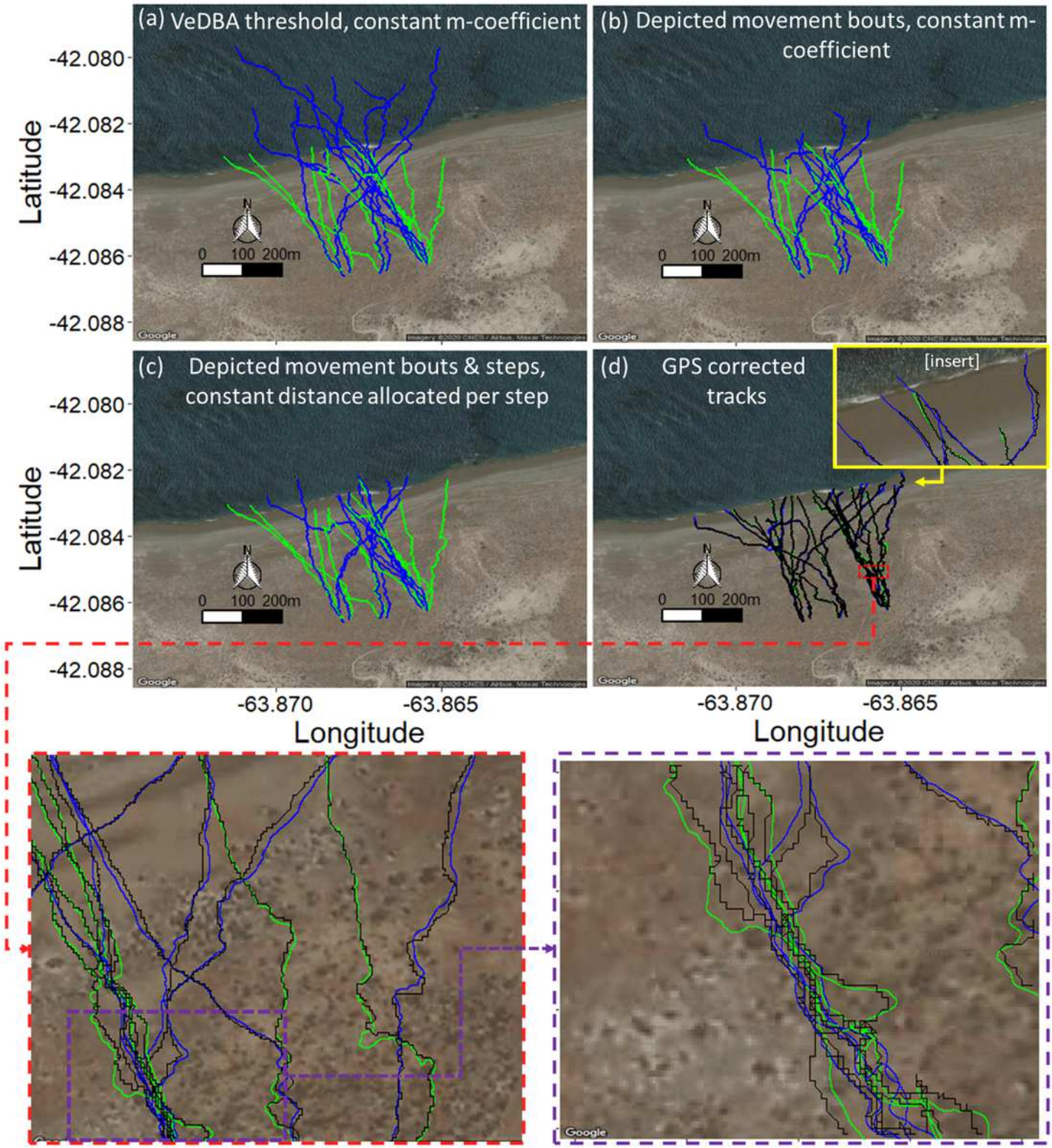

Figure 7

Twelve outgoing (green) and incoming (blue) dead-reckoned trajectories from Magellanic penguins walking to and from their nest. Three variants of track advancement were used; (a) A VeDBA threshold (0.1 g) and constant m-coefficient (1.4) (b), depicted movement periods using the LoCoD method to identify steps (cf. Wilson et al. 2018) and constant m-coefficient (1.4) and (c) depicted individual steps within depicted movement periods, from which a constant distance estimate (0.16 m) was multiplied by

step frequency (x̄ no. steps/s) (full details within SI4) (c). Note that the accuracy with respect to the radial distance can be evaluated by examining the track stops in relation to the shore-line. Tracks (from (c)) were GPS-corrected (d) (method = “distance”, dist.step = 5, VP.ME = TRUE, thresh = between 8-15 (depending on track length)) approx. every 50 m). A portion of the GPS-corrected dead-reckoned tracks (bottom panel) are magnified (2 iterations) to show the difference in resolution of movement tortuosity, between GPS and dead-reckoned tracks. Note: The designations employed and the presentation of the material on this map do not imply the expression of any opinion whatsoever on the part of Research Square concerning the legal status of any country, territory, city or area or of its authorities, or concerning the delimitation of its frontiers or boundaries. This map has been provided by the authors.

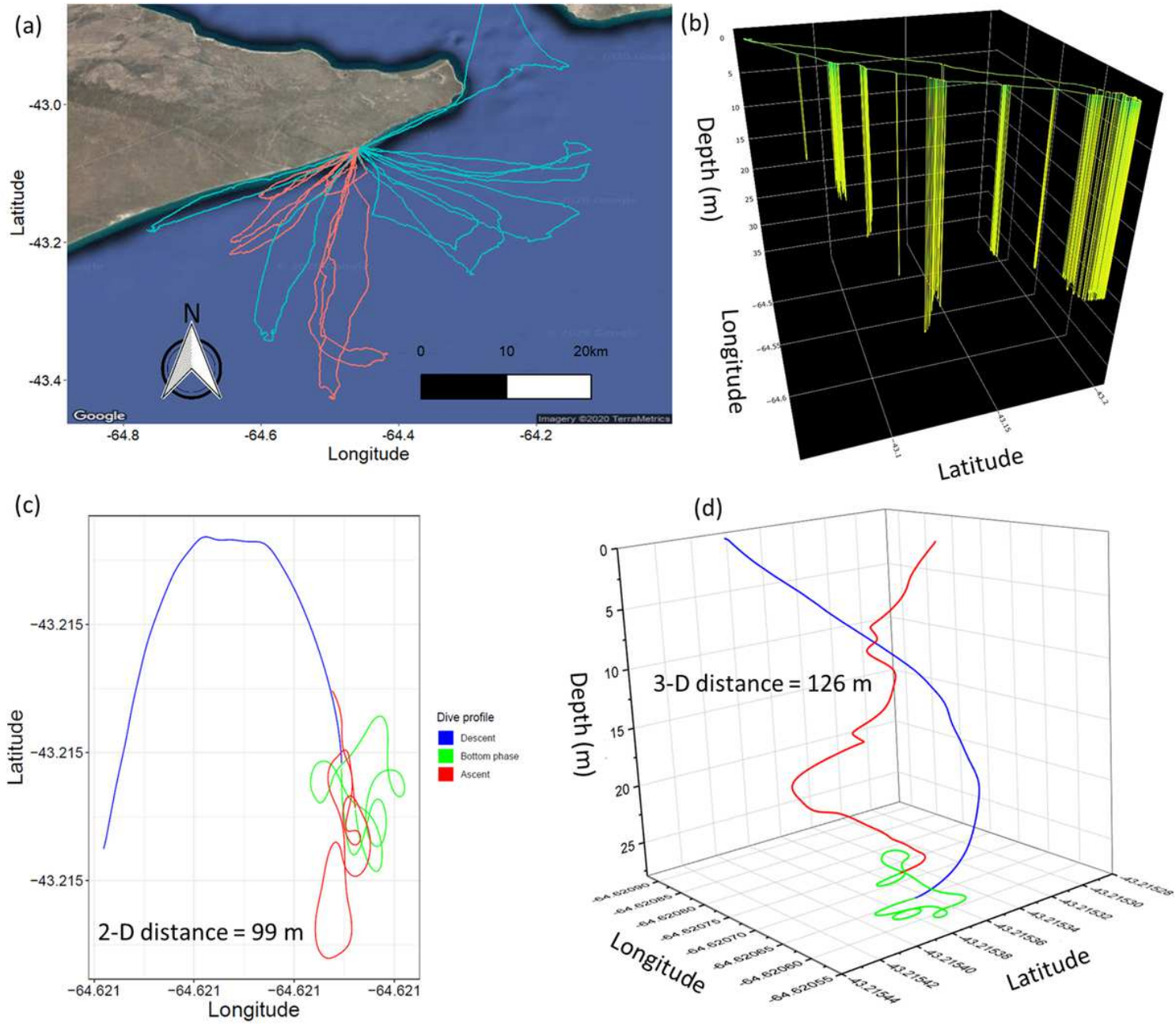

Figure 8

GPS-corrected dead-reckoned tracks of Imperial cormorants foraging at sea; (a) 15 birds (blue = male, red = female). (b) shows one of these tracks illustrated in 3-D. Note gaps between dives are either associated with current drift, while the bird is resting at the sea surface, or periods of flight. (c) and (d) show the descent, bottom phase and ascent of a given dive in both 2-D (c) and 3-D, respectively. Note: The designations employed and the presentation of the material on this map do not imply the expression of any opinion whatsoever on the part of Research Square concerning the legal status of any country, territory, city or area or of its authorities, or concerning the delimitation of its frontiers or boundaries. This map has been provided by the authors.

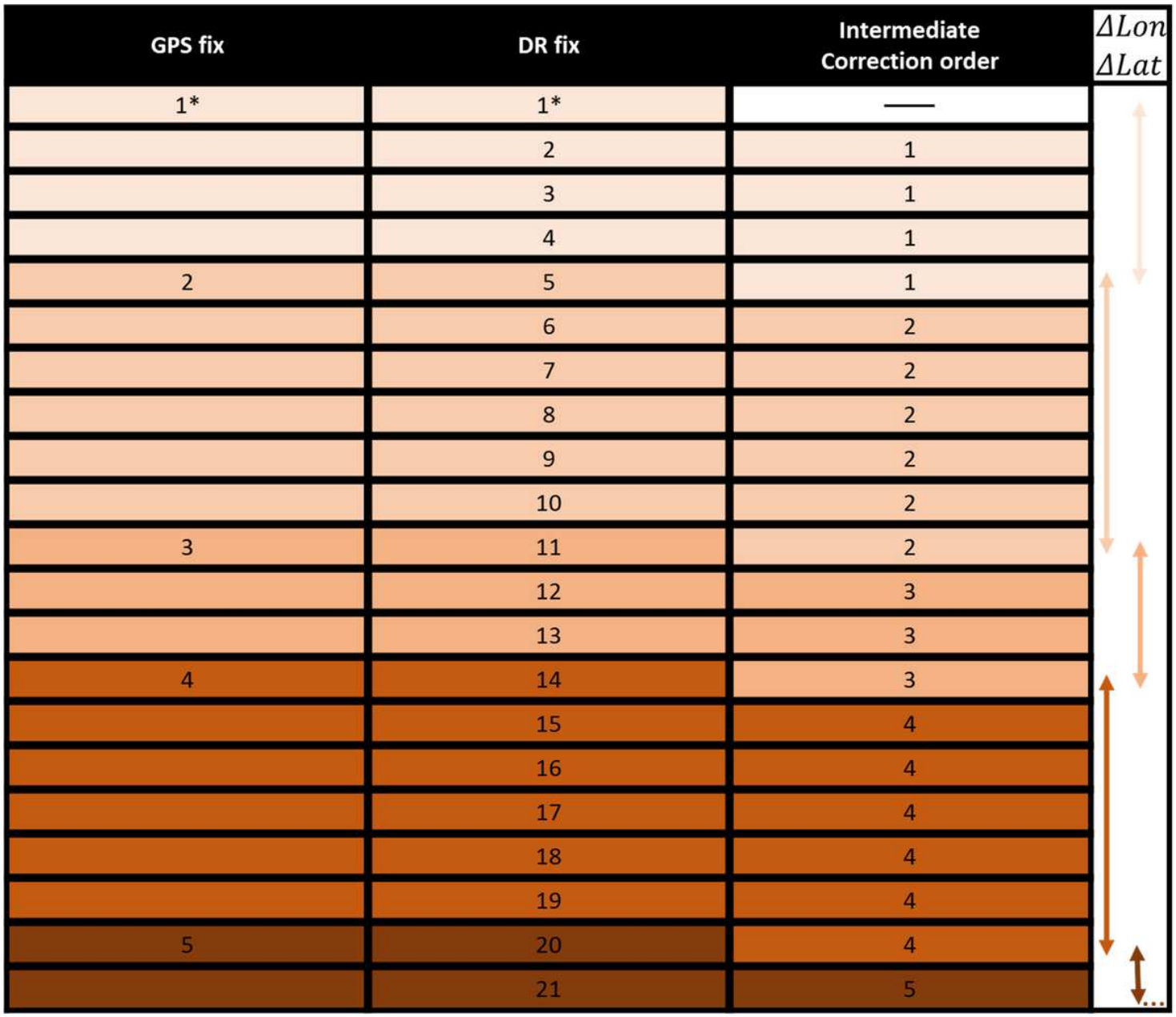

Figure 9

Schematic diagram illustrating the order of fixes used when calculating the □Distance□_(corr.factor) and □Heading□_(corr.factor) (difference of both GPS and dead-reckoned (DR) positions between arrow

heads). Note the discrepancy with the order at which these correction factors are applied to intermediate DR positions (as denoted by colour shading). Known starting position denoted with *.

Supplementary Files

This is a list of supplementary files associated with this preprint. Click to download.

- SI2.Fig.1.png
- SupplementaryInformations.docx
- SI3.Fig.1.png
- SI4.Fig.1.png